DALTON
FULL PAPER

Effect of a halogenide substituent on the stability and photophysical properties of lanthanide triple-stranded helicates with ditopic ligands derived from bis(benzimidazolyl)pyridine †

Carlos Platas Iglesias,[a] Mourad Elhabiri,[a] Marcel Hollenstein,[a] Jean-Claude G. Bünzli[a]* and Claude Piguet[b]

[a] *Institute of Inorganic and Analytical Chemistry, BCH, University of Lausanne, CH-1015 Lausanne, Switzerland. E-mail: jean-claude.bunzli@icma.unil.ch*
[b] *Department of Inorganic, Analytical and Applied Chemistry, University of Geneva, 30 quai E. Ansermet, CH-1211 Geneva 4, Switzerland*

Received 7th March 2000, Accepted 17th May 2000
Published on the Web 15th June 2000

Bis{1-ethyl-2-[6-(*N*,*N*-diethylcarbamoyl)-4-halogenopyridin-2-yl]benzimidazol-5-yl}methane (halogeno = chloro, L^E; bromo, L^F) have been synthesized as ditopic receptors for the development of lanthanide-containing helicates able to couple with biological material and to test the influence of the halogeno substituent on the wrapping process, the structure of the resulting dimetallic edifices, and the photophysical properties of the encapsulated ions. The stability of the $[Eu_2(L)_3]^{6+}$ helicates, as determined by NMR competitive titrations, decreases by respectively one (L^F) and three (L^E) orders of magnitude compared to the value found for the unsubstituted ligand (L^B) although it remains large, log β_{23} = 23.8 (L^F) and 21.8 (L^E) in acetonitrile. The $[Ln_2(L^E)_3]^{6+}$ helicates are shown to be isostructural in acetonitrile over the lanthanide series (Pr to Yb) and the crystal structure of $[Tb_2(L^B)_3]^{6+}$ appears to be a good model for their solution structure, as demonstrated by paramagnetic NMR measurements (lanthanide induced shift method) and relaxation time determination. Ligand L^E appears to be a fair sensitiser of Eu^{III}, the quantum yield of $[Eu_2(L^E)_3]^{6+}$ being 25% larger than that found for $[Eu_2(L^B)_3]^{6+}$, but the ligand $^3\pi\pi^*$ state and $Tb(^5D_4)$ excited level are in resonance, which limits the sensitisation of Tb^{III}. High resolution luminescence spectra of $[Eu_2(L^E)_3]^{6+}$, both in solution and in the solid state, are presented and discussed in terms of site symmetry and vibronic coupling mechanisms.

Introduction

Lanthanide co-ordination compounds[1] are the subject of intense research efforts due to their applications as contrast agents for NMR imaging,[2] as catalysts in RNA hydrolysis,[3] or as active agents in cancer radiotherapy.[4] Moreover, lanthanide-containing luminescent stains[5] are valuable for the development of fluoroimmunoassays[6] and of complexes which signal changes in pH, pO_2 or chloride concentration.[7] A unique combination of features must be realised to design a lanthanide luminescent sensor: (i) presence of multiple absorbing groups suitable for energy transfer (antenna effect[8]), (ii) high thermodynamic and kinetic inertness, and (iii) protection of the metal ion from various quenching or back-transfer processes.[9] Several classes of receptors have been designed to meet these requirements, *e.g.* preorganised[10] and predisposed[11] macrocyclic ligands or multidentate podands.[12] However, self-assembly processes[13] appear to be best suited to achieve the required ultra fine tuning of the lanthanide(III) co-ordination sphere.[14] In recent years we have developed a research program taking advantage of the induced-fit concept[15] and using ligands derived from bis(benzimidazolyl)pyridine in order to prepare lanthanide-containing mono- and di-metallic supramolecular precursors for functional devices.[14] Dimetallic edifices in which lanthanide ions lie at a fixed distance are interesting because they combine two probes in one molecule and are useful for imaging purposes, or they may be used as precursors for doped functional materials requiring the presence of metal ions at a specific distance. The unsymmetrical hexadentate ligands L^I–L^{III} allow the isolation of heterodimetallic non-covalent lanthanide(III) podates $[LnM(L)_3]^{5+}$ (M = Zn,[16] Fe[17] or Co[18]) which are building blocks for luminescent (Zn) and magnetic (Fe, Co) materials. On the other hand, the symmetrical ligands L^A,[19] L^B,[20] and L^C[21] have been synthesized for the self-assembly of homodimetallic cationic helicates $[Ln_2(L^{A,B})_3]^{6+}$ in acetonitrile or highly stable and neutral $[Ln_2(L^C - 2H)_3]$ edifices in water.

Probes for bioanalytical studies require assemblies that are stable under physiological conditions and which can easily couple with biological material. A logical place to introduce a coupling group is the pyridine 4 position of ligands $L^{B,C}$. In this paper we propose an easy strategy to introduce a halogenide substituent in this position, which opens the way for the preparation of more elaborate ligands by substitution of the halogen atom by, for instance, alkyne derivatives.[22] Lamture *et al.* have noted that a 4-Cl substituent increases the energy transfer efficiency in terbium(III) dipicolinates (pyridine-2,6-dicarboxylates)[23] and therefore we devote special attention to the effect of the substitution on the photophysical properties and on the thermodynamics of the complexes. Moreover, we take advantage of the crystal-field independent method applied by Platas *et al.*[24] to monometallic cryptates and recently adapted to dimetallic f–f complexes[25] for the analysis of lanthanide induced paramagnetic NMR shifts.

Results and discussion

Synthesis of ligand L^E

Bis(1-ethyl-2-[4-chloro-6-(*N*,*N*-diethylcarbamoyl)pyridin-2-yl]-benzimidazol-5-yl)methane (L^E) was obtained in good yield according to the previously described two-step procedure

† Electronic supplementary information (ESI) available: analytical, IR and emission spectral data, contact and dipolar shifts, longitudinal relaxation times. See http://www.rsc.org/suppdata/dt/b0/b001818j/

Table 1 ^{1}H NMR shifts (δ, with respect to TMS) for L^E and the $[Ln_2(L^E)_3]^{6+}$ helicates in CD_3CN at 298 K

Compound	H^3	$H^{4'}$	H^5	$H^{7'}$	$H^{6'}$	$H^{10'}$	b-CH_2	$H^{11'}$	H^7	H^9	H^8	H^{10}
L^E [a]	8.42	7.67	7.52	7.35	7.24	4.72	4.27	1.42	3.59	3.35	1.26	1.08
La	8.21	5.95	7.67	7.52	7.27	4.80, 4.68	3.77	1.53	3.47, 3.40	3.07, 2.93	0.96	0.83
Pr	11.10	−8.05	9.38	7.77	6.32	6.43, 5.54	2.49	3.33	4.28, 3.33	2.73, 1.00	1.42	−3.97
Nd	10.07	−0.30	8.88	8.01	6.81	5.56, 5.10	3.13	2.37	3.96, 3.54	2.99, 2.14	1.28	−1.41
Sm	8.40	4.26	7.76	7.43	7.15	4.95, 4.76	3.64	1.69	3.54, 3.37	2.94, 2.67	1.05	0.27
Eu	5.52	12.14	5.89	6.47	7.82	3.09, 2.73	4.55	0.63	4.20, 3.99	3.78, 3.06	0.48	3.27
Tb	17.79	−86.37	13.08	1.11	0.40	[b]	−3.49	13.28	[b]	[b]	5.04	−29.90
Dy	21.45	−99.73	14.60	2.00	−0.96	[b]	−4.68	15.55	[b]	[b]	6.26	−34.92
Ho	16.10	−38.64	12.87	4.09	3.03	[b]	−0.74	9.16	[b]	[b]	3.51	−19.78
Er	7.75	14.31	7.10	7.04	8.69	[b]	4.87	−0.19	[b]	[b]	−0.32	3.19
Tm	4.79	37.16	6.10	8.61	10.52	[b]	6.55	−3.33	[b]	[b]	−1.72	11.18
Yb	6.67	19.62	7.00	7.93	8.65	1.76, 1.17	4.99	−0.63	4.13, 3.14	3.51	−0.04	5.61
Lu	8.29	5.46	7.67	7.53	7.25	4.90, 4.76	3.76	1.53	3.44	2.85	1.11	0.74

[a] In $CDCl_3$. [b] Not assigned.

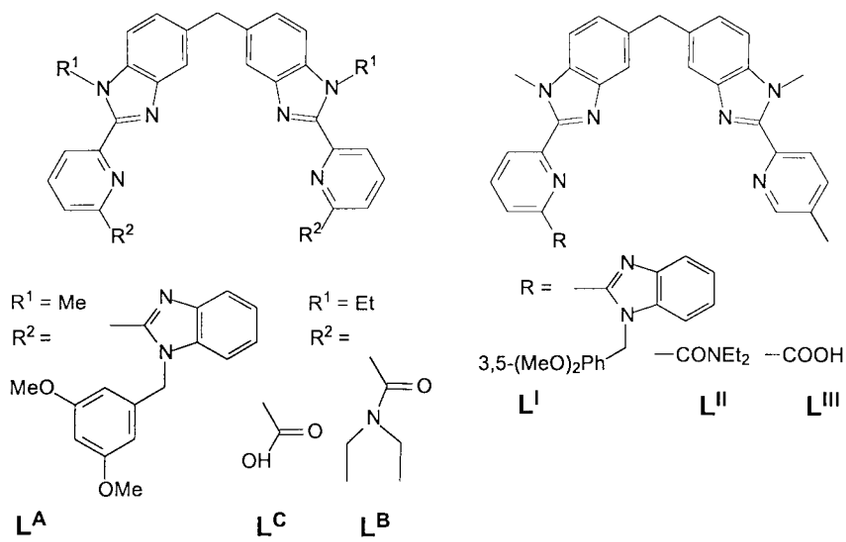

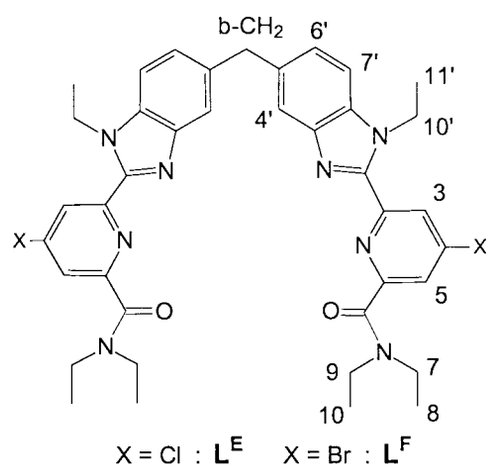

involving a modified Phillips type coupling reaction as the key step in achieving the desired benzimidazole units.[16b] The solution structure of 10^{-2} M L^E in CD_3CN–$CDCl_3$ (5:1) and $CDCl_3$ was investigated by ^{1}H and ^{13}C NMR, including $\{^1H–^1H\}$ COSY experiments (Table 1). The spectra are typical of a species with C_2 symmetry since (i) only 12 proton and 20 carbon signals are observed for the 42 protons and 39 carbon atoms of L^E and (ii) the seven pairs of methylene protons display enantiotopic protons. NOE effects are evidenced between the bridging methylene protons and $H^{4'}$, $H^{6'}$ as well as between $H^{7'}$ and the methylene protons of the ethyl substituent $H^{10'}$, while no such effect is detected between the latter and the aromatic protons of the pyridine unit. This points to a transoid conformation of the two ligand arms, with the *N*-ethyl substituent of the benzimidazole moiety on the same side as the N atom of the pyridine ring. Similar arrangements have been observed previously with tridentate receptors based on bis(benzimidazolyl)pyridine units[26] as well as for L^C.[21]

Preparation and stability of the complexes

Reaction of stoichiometric amounts of L^E and $Ln(ClO_4)_3 \cdot xH_2O$ (Ln = La, Eu, Gd, Tb or Lu) in acetonitrile–dichloromethane mixture gives pale yellow solutions from which the complexes $[Ln_2(L^E)_3][ClO_4]_6 \cdot nH_2O$ (n = 4–10) can be crystallised in 65–80% yield (Table S1, supporting information). These

complexes present a number of identifying IR bands including: (i) an intense carbonyl stretching vibration which is red shifted by 49 cm^{-1} with respect to the "free" ligand, (ii) unco-ordinated H_2O molecules at 3400 cm^{-1} and (iii) typical vibrations from ionic perchlorate at 1090 and 624 cm^{-1}.[27]

In order to get a relative stability scale for the $[Ln_2(L)_3]^{6+}$ helicates with L^B, L^E and L^F, we have performed competitive titrations of the europium complexes with 1,4,10,13-tetraoxa-7,16-diazacyclooctadecane ([2,2]) in a dry CD_3CN–$CDCl_3$ (2.3 : 1) mixture, since the benzimidazole ligands are only sparingly soluble in acetonitrile. The solutions were heated for one week at 45 °C in order to reach thermodynamic equilibrium. The concentrations of the $[Eu_2(L)_3]^{6+}$ helicates and of "free" ligand L were estimated from the ^1H NMR signals of the aromatic protons, the total concentrations of L and [2,2] being *ca.* $5\cdot10^{-3}$ and $2\cdot10^{-4}$ M, respectively and the total concentration in metal ranging between $2.8\cdot10^{-3}$ and $3.1\cdot10^{-3}$ M. It is noteworthy that signals from $[Ln_2(L)_2]^{6+}$ complexes were not detected under these conditions.[20] Defining $[L]_f$ as the concentration of "free" ligand and $[L]_t$ as the total concentration of ligand, we have found $[L]_f/[L]_t = 0.30$, 0.62 and 0.47 for L^B, L^E and L^F, respectively. These data demonstrate that the stability of the helicates decreases gradually in the following sequence: $[Ln_2(L^B)_3]^{6+} > [Ln_2(L^F)_3]^{6+} > [Ln_2(L^E)_3]^{6+}$. That is, the $[Ln_2(L)_3]^{6+}$ helicates become less stable with increasing electronegativity of the substituent introduced in the pyridine 4 position.

The absolute value of the stability constants may be estimated by using log K(Eu[2,2]) = 9.7, as determined in pure CH_3CN,[28] and taking into account a model involving both 2 : 2 and 2 : 3 helicates since these species were shown to form with L^A, L^B, and L^C. We find log β_{22}(Eu) = 20.9 and log β_{23}(Eu) = 25.4 for L^B, log β_{22}(Eu) = 18.3 and log β_{23}(Eu) = 21.8 for L^E, and log β_{22}(Eu) = 19.9 and log β_{23}(Eu) = 23.8 for L^F, where log β_{22}(Eu) and log β_{23}(Eu) are defined by equilibria (1) and (2).

$$2\ Eu^{3+} + 2\ L^{B,E,F} \rightleftharpoons [Eu_2(L^{B,E,F})_2]^{6+} \quad \log \beta_{22}(Eu) \quad (1)$$

$$2\ Eu^{3+} + 3\ L^{B,E,F} \rightleftharpoons [Eu_2(L^{B,E,F})_3]^{6+} \quad \log \beta_{23}(Eu) \quad (2)$$

Although these data can only be taken as an estimate (evaluated error: ±1.5 to 2), the experimental conditions employed not being entirely the same, the results obtained for L^B are in very good agreement with those determined previously by a direct spectrophotometric method (log β_{22}(Eu) = 19.9 and log β_{23}(Eu) = 24.1).[20]

Solution structure of $[Ln_2(L^E)_3]^{6+}$ in acetonitrile

The ^1H NMR spectra of the lanthanum and lutetium diamagnetic complexes (Table 1) show an A_2 spin system for the bridging b-CH_2 group, which is typical for C_2-related enantiotopic protons, while the *AB* spin system observed for methylene protons $H^{10'}$ arises from two symmetrically non-equivalent diastereotopic protons, leading to the conclusion that the helicates adopt a time-averaged D_3 symmetry on the NMR timescale.[16,20] The complete assignment of the spectra was made on the basis of homodinuclear {^1H–^1H}-COSY and {^1H–^1H}-ROESY (rotating frame Overhauser enhancement spectroscopy) experiments. Analysis of the spectra reveals that the ionic radius contraction does not modify substantially the overall structure of the helicates. However, the signal of the $H^{4'}$ protons is shifted by +0.48 ppm in going from La to Lu, pointing to some distortion in the co-ordination sphere of the heavier metal ion.[20] This proton experiences a large shift upon complexation ($\Delta\delta$ = +1.74 and +2.22 ppm for La and Lu, respectively) because the peculiar conformation of the helicates brings it in the shielding zone of the benzimidazole units.[19,20] The pyridine protons also undergo substantial shifts as a result

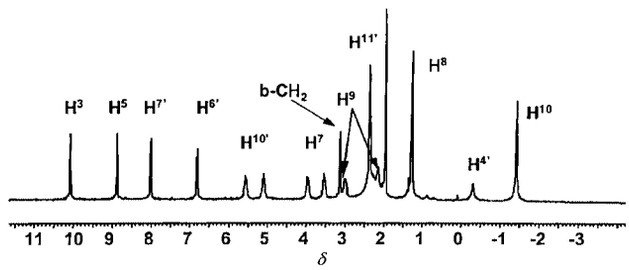

Fig. 1 360 MHz ^1H NMR spectrum of $[Nd_2(L^E)_3]^{6+}$ in CD_3CN at 295 K.

of (i) the co-ordination of the pyridine N atom to the metal ions and (ii) the conformational change from a transoid to a cisoid arrangement of the two arms of the ligand. The latter conformation is confirmed by the NOE effect detected for the lanthanum helicate between $H^{10'}$ and H^3. The spectra of the moderately paramagnetic helicates (Ln = Pr, Nd, Sm, Eu or Yb) also display an A_2 spin system for the b-CH_2 protons and an *AB* system for the $H^{10'}$ protons, corresponding to a time-averaged D_3 symmetry in solution (Fig. 1). For the samarium helicate, which displays very small isotropic shifts and sharp signals, assignments could be made referring to the spectrum of the diamagnetic lanthanum helicate while the spectra of the complexes of Nd and Eu were assigned with the help of {^1H–^1H}-COSY and {^1H–^1H}-ROESY spectra. For strongly paramagnetic lanthanide complexes resonance assignments were made on the basis of signal integration, linewidth analyses and the results obtained for the complexes of Pr and Eu.

Finer structural information can be gained from the separation of the contact (δ_{ij}^c) and pseudocontact contributions (δ_{ij}^{pc}) to the isotropic paramagnetic shift (δ_{ij}^{para})[29] of a nucleus *i* induced by a lanthanide ion *j* (LIS), eqn. (3) where the diamagnetic

$$\delta_{ij}^{para} = \delta_{ij}^{exp} - \delta_i^{dia} = \delta_{ij}^c + \delta_{ij}^{pc} \quad (3)$$

contribution δ_i^{dia} is obtained by measuring chemical shifts for isostructural diamagnetic complexes: $[La_2(L^E)_3]^{6+}$ was used for the earlier (Pr to Dy) and $[Lu_2(L^E)_3]^{6+}$ for the later (Ho to Yb) members of the lanthanide series. Equations have recently been developed for homodimetallic complexes with large Ln···Ln separation (8–9 Å) in which pseudocontact contributions affect the LIS of protons which are significantly remote from the paramagnetic centre.[21b] For axial lanthanide complexes[30] the pseudocontact contribution is given by eqn. (4) where $A_2^0\langle r^2\rangle$ is

$$\delta_{ij}^{pc} = \sum_{n=1}^{2} \frac{(A_2^0\langle r^2\rangle)^n}{T^2}\cdot\left(\frac{1-3\cos^2\theta_i^n}{(r_i^n)^3}\right)\cdot C_j^n = \sum_{n=1}^{2} G_i^n C_j^n \quad (4)$$

the crystal field parameter, C_j^n the anisotropic part of the axial magnetic susceptibility tensor, r_i^n and θ_i^n are the internal axial coordinates of nucleus *i* with respect to the threefold axis of site *n* and G_i^n is the pseudocontact term originating from ion *n* at a given temperature. On the other hand, the contact contributions δ_{ij}^c only affect nuclei relatively close to the paramagnetic centre and it can be assumed that in the helicates $[Ln_2(L^E)_3]^{6+}$ they result from the interaction with a single metal ion. Under these conditions, and assuming that the paramagnetic centres do not interact in view of their large separation, the linearised equations (5)–(7) hold[21b] where $\langle S_z\rangle_j$ is the spin expectation

$$\frac{\delta_{ij}^{para}}{\langle S_z\rangle_j} = F_i + G_i^{global}\frac{C_j}{\langle S_z\rangle_j} \quad (5)$$

$$\frac{\delta_{ij}^{para}}{C_j} = G_i^{global} + F_i\frac{\langle S_z\rangle_j}{C_j} \quad (6)$$

Table 2 Computed values for contact (F_i) and pseudocontact (G_i^{global}) terms and agreement factors AF_i and AF_j for ^1H nuclei in $[Ln_2(L^E)_3]^{6+}$ in CD_3CN solution[a]

	b-CH_2	$H^{4'}$	$H^{6'}$	$H^{7'}$	H^3	H^5	$H^{11'}$	H^{10}	H^8
Pr to Dy									
$\theta_i^1/°$ [a]	53.15	39.84	53.13	58.81	81.55	109.21	83.14	140.28	111.38
r_i^1/Å [a]	6.634	3.917	7.019	6.755	5.476	5.420	6.618	5.515	6.613
$\theta_i^2/°$ [a]	46.28	22.41	49.12	46.04	33.16	24.13	38.53	14.26	26.84
r_i^2/Å [a]	7.349	6.556	7.427	8.015	9.862	11.974	10.513	13.605	12.998
F_i [b]	−0.049(1)	−0.23(3)	−0.025(3)	0.144(6)	0.245(6)	0.170(5)	0.039(3)	−0.116(6)	0.031(7)
G_i^{global} [b]	−0.101(1)	−1.17(2)	−0.085(2)	−0.017(2)	0.199(1)	0.116(3)	0.153(1)	−0.399(3)	0.049(5)
F_i/G_i^{global} [b]	0.49	0.19	0.29	−8.47	1.23	1.47	0.25	0.29	0.63
AF_i [b]	0.0239	0.0346	0.0519	0.0557	0.0263	0.0940	0.0124	0.02036	0.2237
F_i [c]	0.000	0.000	0.000	0.156	0.412	0.382	0.000	0.126(8)	0.09
G_i^{global} [c]	−0.078	−1.06	−0.053	−0.013	0.261	0.195	0.149(3)	−0.307(7)	0.083(2)
AF_i [c]	0.0757	0.0018	0.3377	0.000	0.000	0.000	0.0801	0.000	0.000
Ho to Yb									
F_i [b]	0.080(4)	0.1(2)	0.062(1)	0.098(4)	−0.20(1)	−0.143(3)	−0.138(2)	0.434(9)	−0.0164
G_i^{global} [b]	−0.066(1)	−0.73(2)	−0.0711(4)	−0.031(3)	0.097(1)	0.049(2)	0.1142(9)	−0.270(4)	0.055(1)
F_i/G_i^{global} [b]	−1.21	−0.14	−0.87	−3.16	−2.06	−2.92	−1.21	−1.61	−0.30
AF_i [b]	0.0361	0.3551	0.0125	0.0635	0.0949	0.0351	0.0118	0.0175	0.0447
G_i^{global} [c]	−0.045	−0.61	−0.03	−0.01			0.09		0.048
	Pr	Nd	Eu	Tb	Dy	Ho	Er	Tm	Yb
AF_j [b]	0.0322	0.0474	0.0681	0.0160	0.0442	0.0223	0.1882	0.0315	0.0209
AF_j [c]	0.0245	0.0314	0.0516	0.0256	0.0270			0.0588 [d]	0.0523 [d]
AF_j [e]	0.136	0.113	0.251	0.190	0.1746	0.203	0.381	0.187	0.187

[a] Averaged axial coordinates r_i^n and θ_i^n tabulated from the crystal structure of the $[Tb_2(L^B)_3]^{6+}$ helicate. [b] According to Reilley's method. [c] According to Kemple's method. [d] According to the dipolar model excluding H^3, H^5 and H^{10} from the fits. [e] According to the dipolar model.

$$AF_i = [\sum_j (\delta_{ij}^{exp} - \delta_{ij}^{cal})^2 / \sum_j (\delta_{ij}^{exp})^2]^{1/2} \quad \text{and}$$

$$AF_j = [\sum_i (\delta_{ij}^{exp} - \delta_{ij}^{cal})^2 / \sum_i (\delta_{ij}^{exp})^2]^{1/2} \quad (7)$$

value and F_i the contact term at fixed temperature. Assuming further that $\langle S_z \rangle_j$ and C_j values are the same for the complexes and the free ions,[31] for which they are tabulated,[32,33] plots of $\delta_{ij}^{para}/\langle S_z \rangle$ against $C_j/\langle S_z \rangle$ and of δ_{ij}^{para}/C_j against $\langle S_z \rangle/C_j$ should be linear with a slope equal to $G_i^{global} = G_i^1 + G_i^2$ and F_i, respectively, if the complexes are isostructural and possess comparable crystal field parameters. The pseudocontact and contact contributions to the observed LIS separated by using eqns. (5) and (6) are reported in Table 2 along with the agreement factors AF_i and AF_j (see also Table S2, supporting information). The diastereotopic methylene protons of the ethyl substituents have been excluded from the analysis because a reliable assignment is not possible for an *AB* spin system.[21b] We have also not used samarium data in our calculations because the shifts induced by this ion are small and extremely temperature dependent. The resulting plots fall into two groups (Ln = Pr to Dy and Ln = Ho to Yb) with a break near the middle of the series as illustrated in Fig. 2 for H^{10}. In principle, such a situation points to the $[Ln_2(L^E)_3]^{6+}$ helicates being not isostructural. However, deviations from linearity sometimes occur because of variation in the crystal field parameter[34] or in both this parameter and the hyperfine coupling constant F_i.[24] The agreement factors calculated for both series, $0.012 < AF_i < 0.22$ (Pr to Dy) and $0.01 < AF_i < 0.36$ (Ho to Yb), are comparable to those found for the 3d–4f helicates $[LnZn(L)_3]^{5+}$ with $L = L^I$ (0.08–0.27),[16a] L^{II} (0.07–0.20),[16b] or for $[Ln_2(L^C - 2H)_3]$ ($0.0015 < AF_i < 0.35$).[21b] The contact contributions are relatively small for most of the protons in the first half of the series (Ln = Pr to Tb), F_i reaching significant values only for $H^{4'}$, H^3, H^5, $H^{7'}$, and H^{10}. The large F_i values calculated for the H^3 and H^5 protons for both series point to an important spin density delocalisation onto the pyridine ring. However, these values are smaller than those obtained previously for $[LnZn(L)_3]^{5+}$, with $L = L^I$ (0.34, 0.34)[16a] or L^{II} (0.35, 0.22),[16b] and for $[Ln_2(L^C - 2H)_3]$ (0.32, 0.36 for Ce to Tb and −0.47, −0.46 for Er to Yb),[21b] pointing to a reduced spin density delocalisation on the pyridine rings, as a consequence of the electronegative substituent.

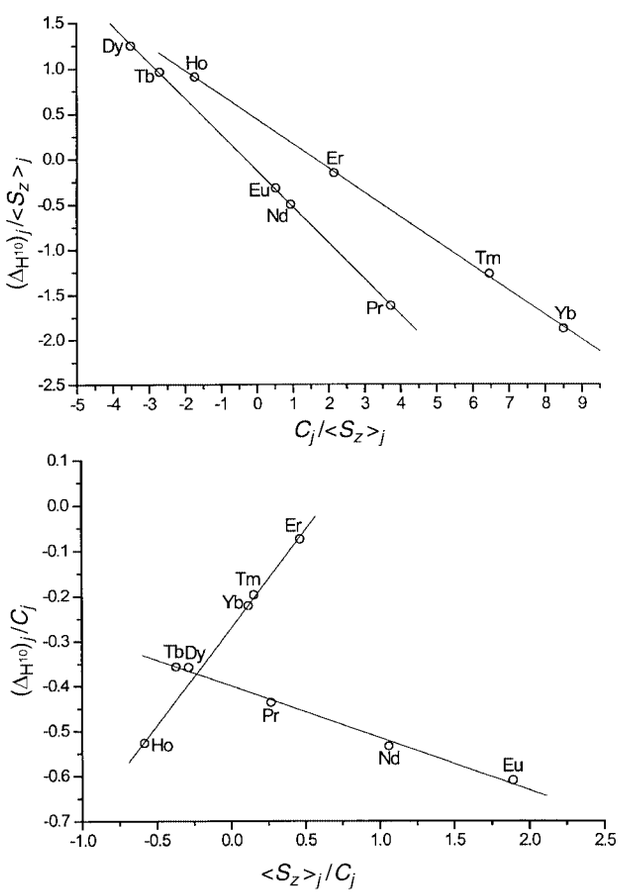

Fig. 2 Plots according to eqns. (5) and (6) for the H^{10} protons.

Recently, Platas *et al.*[24] proposed a crystal-field independent method, which allows one to rationalise the origin of the breaks

Table 3 Geometric ratios R_{ik} and intercepts $(F_i - R_{ik}F_k)$ for $[Ln_2(L^E)_3]^{6+}$ (CD_3CN, 298 K)

	b-CH_2–$H^{4'}$	b-CH_2–$H^{6'}$	b-CH_2–$H^{11'}$	b-CH_2–H^{10}	$H^{4'}$–$H^{11'}$	$H^{4'}$–H^{10}	$H^{4'}$–$H^{6'}$	$H^{11'}$–H^{10}	$H^{6'}$–$H^{10'}$	$H^{6'}$–H^{11}	
Pr to Yb											
R_{ik}[a]	0.087(2)	0.94(4)	−0.61(2)	0.249(3)	−7.9(4)	2.86(8)	10.8(5)	−0.41(1)	0.25(2)	−0.61(2)	
$(F_i - R_{ik}F_k)$[a]	−0.013(7)	0.01(1)	−0.008(9)	−0.018(3)	−0.2(2)	−0.11(9)	$H^{4'}$–$H^{11'}$	0.03(1)	−0.02(2)	−0.01(1)	
Pr to Dy											
R_{ik}[b]	0.086	1.19	−0.66	0.253	−7.65	2.93	13.76	−0.38	0.21	−0.56	
Ho to Yb											
R_{ik}[b]	0.090	0.93	−0.58	0.244	−6.39	2.70	10.27	−0.42	0.26	−0.62	
	b-CH_2–H^3	b-CH_2–H^5	H^3–$H^{4'}$	H^5–$H^{4'}$	H^3–H^{10}	H^5–H^{10}	$H^{11'}$–H^3	H^5–H^3	$H^{11'}$–H^5	$H^{6'}$–H^5	$H^{6'}$–H^3
Pr to Dy											
R_{ik}[a]	−0.507(7)	−0.87(2)	−0.170(3)	−0.099(3)	−0.499(7)	−0.290(7)	0.767(4)	0.58(1)	1.32(2)	−0.73(1)	−2.34(5)
$(F_i - R_{ik}F_k)$[a]	0.069(4)	0.087(6)	0.18(1)	0.127(9)	0.174(7)	0.121(7)	−0.136(2)	0.020(6)	−0.162(7)	0.010(4)	0.20(1)
R_{ik}[b]	−0.508	−0.87	−0.17	−0.099	−0.499	−0.291	0.769	0.58	1.32	−0.73	−2.34
Ho to Yb											
R_{ik}[a]	−0.67(6)	−1.34(7)	−0.134(6)	−0.067(6)	−0.36(4)	−0.18(1)	1.16(8)	0.51(3)	2.3(1)	−1.45(6)	−1.37(9)
$(F_i - R_{ik}F_k)$[a]	−0.07(2)	−0.11(1)	−0.11(2)	−0.09(2)	0.07(5)	−0.07(2)	0.11(4)	−0.04(3)	1.20(2)	−0.15(1)	−0.13(3)
R_{ik}[b]	−0.68	−1.35	−0.133	−0.067	−0.36	−0.18	1.18	0.51	2.3	−1.45	−1.36

[a] According to eqn. (8). [b] According to eqns. (5) and (6).

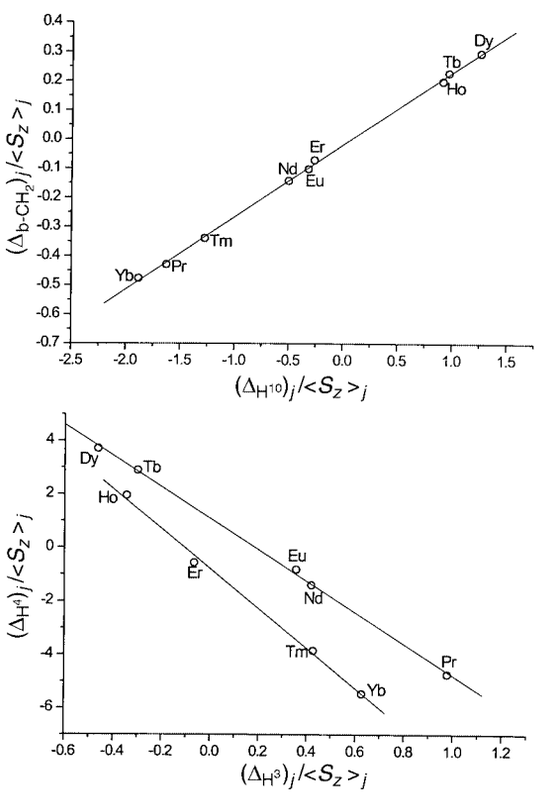

Fig. 3 Plots according to eqn. (8) for the pairs b-CH_2–H^{10} (top) and $H^{4'}$–H^3 (bottom).

found in the plots according to eqns. (5) and (6), by simultaneously solving eqn. (3) for two different nuclei i and k. Its extension to dimetallic helicates leads to eqn. (8).[25] The corresponding plots for the studied helicates present three different behaviours depending on the protons. (i) Pairs involving $H^{4'}$, $H^{6'}$, $H^{11'}$, H^{10} and b-CH_2 display a single straight line (Pr to Yb, Fig. 3) indicating that changes in the crystal field parameter are responsible for the break observed between Dy and Ho (Fig. 2), rather than structural variation, and that these protons have similar hyperfine coupling constants with all the studied lanthanide ions, consistent with a single structure along the series. (ii) On the other hand, plots for the pairs involving the H^8 and $H^{7'}$ protons do not show obvious correlation, which can be explained by the low G^{global} values (Table 2) inducing large errors in $G_i^{global}/G_k^{global}$. (iii) Finally, plots for pairs involving H^3 and H^5 clearly show two approximately parallel straight lines, one for the larger (Pr to Dy) and one for the smaller (Ho to Yb) ions which implies a significant change in the hyperfine coupling constants for these protons in the two series. This intricate behaviour can be explained if one compares the contact contributions obtained by Reilley's method (Table 2), which display important variations between the first and second half of the lanthanide series. However, the contact contribution and/or the contact to dipolar quotient (F_i/G_i^{global}) are relatively small for most of the protons, except for H^3 and H^5. Thus, the plots according to eqn. (8) for the latter protons are very sensitive to changes in the hyperfine coupling constant.

$$\frac{\delta_{ij}^{para}}{\langle S_z\rangle_j} = (F_i - R_{ik}F_k) + R_{ik}\frac{\delta_{kj}^{para}}{\langle S_z\rangle_j}, \quad R_{ik} = G_i^{global}/G_k^{global} \quad (8)$$

Turning our attention to the R_{ik} values (Table 3) we note that for pairs generating a single straight line the values obtained according to both Reilley's and the crystal-field independent methods are in excellent agreement. For the pairs generating two lines, the R_{ik} values for the first and second half of the series are in qualitative good agreement, pointing to a minor structural change in the pyridine units between the helicates of Dy and Ho. Furthermore, a plot of G_i^{global} (Ho to Yb) *vs.* G_i^{global} (Pr to Dy) for all protons generates a straight line going through the origin with a slope of 0.62(2) ($R^2 = 0.997$), indicating that the G_i^{global} values for the first and second part of the lanthanide series differ only by a proportionality constant assigned to a change in the crystal field parameter between Dy and Ho. We conclude that the solution structure of the helicates is essentially maintained along the series and that the breaks found between Dy and Ho in the plots according to eqns. (5) and (6) are due to changes in the crystal field parameter and in the hyperfine coupling constant as similarly discussed for $[Ln_2(L^C - 2H)_3]$ in water.[25]

Substitution of Bleaney's coefficients C_j by a direct determination of the magnetic susceptibility tensor[35] considerably improves the separation of the contact and dipolar contributions to the LIS. To calculate the latter, the axial coordinates

r_i^n and θ_i^n ($n = 1$ or 2) of the protons b-CH_2, $H^{4'}$, $H^{6'}$, $H^{7'}$, H^3, H^5, $H^{11'}$, H^8 and H^{10} need to be determined. As it is reasonable to assume that the introduction of a chloride substituent does not affect substantially the structure of the helicates, we have calculated the axial coordinates from the crystal structure of $[Tb_2(L^B)_3]^{6+}$ [20] using the Tb–Tb pseudo-threefold axis as the magnetic z axis. LIS values have been first fitted by eqn. (9)

$$\delta_{ij}^{para} = \xi\chi_j^{zz}\left(\frac{1 - 3\cos^2\theta_i^1}{(r_i^1)^3} + \frac{1 - 3\cos^2\theta_i^2}{(r_i^2)^3}\right) + \sum_i \delta_{ij}^{c} \quad (9)$$

without including the contact contributions. As expected, these fits were rather poor (*cf.* the large agreement factors, Table 2). A much better agreement ($0.025 < AF_j > 0.052$) was obtained for the first half of the series when contact contributions for $H^{7'}$, H^3, H^5, H^8 and H^{10} were treated as fitting parameters. Thus, the mathematical treatment employed required the calculation of five parameters for each lanthanide ion in addition to the experimental axial anisotropic susceptibility parameter $\xi\chi_j^{zz}$ (9×6 fit). Although the improvement obtained should be considered with caution because adding new fitting parameters lowers the AF_j values,[36] the calculated contact and dipolar contributions obtained from both Reilley's and Kemple's methods are in qualitative agreement (Table 2, Tables S2 and S3, supporting information), except for the contact contribution for H^{10}. We conclude that the solid state structure of $[Tb_2(L^B)_3]^{6+}$ is a good model for the solution structure of the helicates of Pr to Dy with L^E. This statement is confirmed by the good match observed between the theoretical C_j values and the experimental axial component of the anisotropic susceptibility (Table 4).

For the second half of the series (Ln = Ho to Yb) the contact contributions are dominant for most of the protons and this mathematical treatment could not successfully be employed. The theoretical values for the ratio of the contact to dipolar contributions to the isotropic shifts should be of the order of $-0.58:0.47:0.15:0.12$ for an isostructural series of complexes of trivalent Ho, Er, Tm and Yb. Thus, good fits, according to the dipolar model, are expected for Tm and Yb only, which is indeed the case when the H^3, H^5 and H^{10} protons having the largest contact to dipolar ratio (Table 2) are excluded from the fits. Furthermore, the dipolar contributions calculated by this method are in good agreement with those obtained by Reilley's method (Table 2). We conclude that the solid state structure of $[Tb_2(L^B)_3]^{6+}$ is also a good model for the solution structure of the $[Ln_2(L^E)_3]^{6+}$ helicates with the heavier lanthanide ions and that no drastic structural change occurs for the L^E complexes along the lanthanide series.

Further structural information can be obtained by measuring the NMR longitudinal relaxation times T_1. The effects of the paramagnetic centre on T_1 are accounted for by the Solomon–Bloembergen–Morgan theory,[37] which reduces to dipolar and Curie-spin contributions, depending on r_i^{-6}, for lanthanide complexes.[29] The use of a nucleus sufficiently remote from the paramagnetic centre as an internal reference gives eqn. (10) in

$$\frac{k_{ref}^{tot} - k_{ref}^{dia}}{k_i^{tot} - k_i^{dia}} = \left(\frac{r_i}{r_{ref}}\right)^6 \quad (10)$$

which k_i^{tot} and k_i^{dia} are the longitudinal relaxation rates measured for the nucleus i in the paramagnetic complex and its diamagnetic analogue, respectively. For dimetallic helicates the T_1 of each nucleus is the sum of two dipolar paramagnetic contributions,[21b] eqn. (11). The relaxation times of the paramagnetic

$$\frac{k_{ref}^{tot} - k_{ref}^{dia}}{k_i^{tot} - k_i^{dia}} = \left(\frac{(r_{ref}^1)^6 + (r_{ref}^2)^6}{(r_i^1)^6 + (r_i^2)^6}\right) + \left(\frac{(r_i^1)^6(r_i^2)^6}{(r_{ref}^1)^6\,(r_{ref}^2)^6}\right) \quad (11)$$

$[Ln_2(L^E)_3]^{6+}$ complexes (Ln = Pr or Yb), corrected for diamagnetic contribution using the values for the helicates of La and Lu, are reported in Table 5 (uncorrected values; Table S4, supporting information). Taking the r_i^n distances from the crystal structure of $[Tb_2(L^B)_3]^{6+}$ (Table 2) and H^8 as an internal reference, we have estimated the expected quotients $(k_{ref}^{tot} - k_{ref}^{dia})/(k_i^{tot} - k_i^{dia})$. The differences between the two approaches (eqns. (10) and (11)) are minor for protons H^3, H^5, H^8, H^{10} and $H^{4'}$ (<2.5%) because r_i^1 and r_i^2 are sufficiently different and the contribution of one paramagnetic centre dominates. Eqn. (10) can thus be used to extract the approximate Ln···H distances collected in Table 5. The experimental distances obtained from the relaxation data of the complexes of Pr and Yb are in excellent agreement, which confirm again that there is no important structural change along the series. Moreover, a comparison of the experimental $[(k_{ref}^{tot} - k_{ref}^{dia})/(k_i^{tot} - k_i^{dia})]_{exp}$ values obtained from the relaxation measurements with those calculated from the crystal structure of the $[Tb_2(L^B)_3]^{6+}$ helicate shows a satisfying concordance for all the protons except for H^{10}.

Table 4 Comparison of theoretical (C_j) and experimental ($\xi\chi_j^{zz}$/ppm Å^3) values of the axial component of the anisotropic susceptibility for $[Ln_2(L^E)_3]^{6+}$

Ln	C_j	$\xi\chi_j^{zz}$	C_j/C_{Pr}	$\xi\chi_j^{zz}/\xi\chi_{Pr}^{zz}$
Pr	−11.00	−761	1.00	1.000
Nd	−4.20	−342	0.38	0.45
Eu	4.00	339	−0.364	−0.44
Tb	−86.00	−5022	7.82	6.60
Dy	−100	−5753	9.09	7.56

Photophysical properties

Ligand-centred transitions. The emission spectrum of L^E in acetonitrile solution (295 K) under excitation at 31 546 cm^{-1} presents a single band (Table 6) whose intensity quickly diminishes when a short time delay (0.1 ms) is enforced and therefore has been attributed to the $^1\pi\pi^*$ state. This band is shifted by *ca.* 1550 cm^{-1} to higher energy with respect to that of L^B. The absolute fluorescence quantum yield is large and amounts to $Q^L = 92\%$. The emission spectrum recorded in frozen solution

Table 5 Ln···H distances in CD_3CN $[Ln_2(L^E)_3]^{6+}$ solutions calculated from corrected experimental relaxation times (T_1) and normalised to the Tb···H^8 distance

Ln		b-CH_2	$H^{6'}$	$H^{7'}$	$H^{11'}$	$H^{4'}$	H^3	H^5	H^{10}	H^8
Pr	T_1/ms	[a]	[a]	623.4	[a]	25.91	190.0	180.7	156.1	766.5
	r_i^1/Å					3.76	5.25	5.21	5.06	6.61
Yb	T_1/ms	226.9	259.5	259.4	189.1	8.41	84.4	72.2	52.7	257.43
	r_i^1/Å					3.75	5.50	5.35	5.06	6.61
Tb[b]	r_i^1/Å	6.63	7.02	6.76	6.62	3.91	5.48	5.42	5.52	6.61
Pr	$[(k_{ref}^{tot} - k_{ref}^{dia})/(k_i^{tot} - k_i^{dia})]_{exp}$ [c]	[a]	[a]	0.81	[a]	0.034	0.25	0.24	0.20	1
Yb	$[(k_{ref}^{tot} - k_{ref}^{dia})/(k_i^{tot} - k_i^{dia})]_{exp}$ [c]	0.88	1.01	1.01	0.73	0.033	0.33	0.28	0.20	1
Tb[b]	$[(k_{ref}^{tot} - k_{ref}^{dia})/(k_i^{tot} - k_i^{dia})]_{calc}$ [c]	0.67	0.85	0.85	0.96	0.042	0.32	0.31	0.34	1

[a] Overlapping of some peaks prevents the T_1 measurement. [b] From the crystal structure of $[Tb_2(L^B)_3]^{6+}$. [c] According to eqn. (11) with H^8 as an internal reference, see text.

Table 6 Ligand-centred absorption and emission properties of L^E and $[Ln_2(L^E)_3]^{6+}$

Compound	$\pi \longrightarrow \pi^*$ [a]	$\pi \longrightarrow \pi^*$ [b]	$^1\pi\pi^*$ [c]	$^3\pi\pi^*$ [c]	$\tau(^3\pi\pi^*)$ [c]
L^E	29 420 (sh)	28 484	25 883	16 806	670 ± 20
	30 841 (4.77)	41 298		18 957	
	40 160 (4.51)			21 199	
La	29 710 (5.10)	26 232	22 730	18 860	587 ± 30
	40 095 (5.03)	40 955		19 860	
	47 820 (5.45)	47 567		20 860	
Eu	29 480 (5.10)	25 976		[d]	[d]
	39 940 (5.04)	41 857			
	48 080 (5.41)	48 121			
Gd		26 438	22 821	17 946	5.3 ± 0.1
		41 857		19 219	
		47 463		20 455	
Tb	29 520 (5.10)	26 193		[d]	[d]
	39 900 (5.02)	40 838			
	47 820 (5.42)	47 633			
Lu		26 407	22 245	18 388	146 ± 5
		41 088		18 999	
		47 592		20 337	

[a] Electronic spectral data in acetonitrile at 295 K; energies are given for the maximum of the band envelope in cm^{-1}, and log ε is given within parentheses. [b] Reflectance spectra recorded at 295 K. [c] Luminescence data and lifetimes (ms) in frozen CH_3CN solutions at 77 K. [d] $^3\pi\pi^*$ luminescence quenched by transfer to the lanthanide ion.

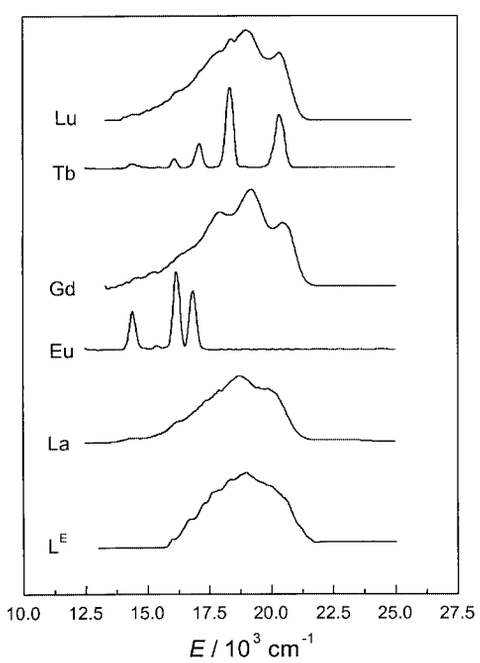

Fig. 4 Corrected phosphorescence spectra of L^E and the $[Ln_2(L^E)_3]^{6+}$ helicates at 77 K (ν_{exc} = 26 316 cm^{-1}). Vertical scale: arbitrary units.

(77 K) presents a second more structured band with a maximum at 18 957 cm^{-1} and with a number of low- and high-energy shoulders (Fig. 4). This band has a single exponential time decay with a lifetime of 670 ± 20 ms and is therefore assigned to the $^3\pi\pi^*$ state. This lifetime is considerably longer than the one reported for L^A (4.4 ms[19]) and L^B (4.2 ms[20]), which should promote efficient ligand-to-metal energy transfer processes.

In acetonitrile the $[Ln_2(L^E)_3]^{6+}$ helicates display three main absorption bands at 48 000, 40 000 and 29 500 cm^{-1} assigned respectively to $\pi \longrightarrow \pi^*$ transitions mainly located on the carbonyl, pyridine and benzimidazole moieties. The low energy band undergoes a red shift of 1360 cm^{-1} upon complexation. Similarly, the ligand-based singlet state emission band shifts to lower energies in the helicates of La^{III}, Gd^{III} and Lu^{III} and the energy of the 0-phonon transition of the $^3\pi\pi^*$ state undergoes an increasing bathochromic shift with increasing charge density of the metal ion: 339 (La), 744 (Gd) and 858 (Lu) cm^{-1}.

$[Eu_2(L^E)_3]^{6+}$ helicate in acetonitrile solution. The excitation spectrum of a $7\cdot10^{-4}$ M solution of $[Eu_2(L^E)_3]^{6+}$ in acetonitrile produces a broad and intense band with a maximum at 25 200 cm^{-1}, corresponding to excitation through the $^1\pi\pi^*$ ligand state. The corresponding emission spectrum points to the complexes having an averaged trigonal symmetry in solution, in agreement with the NMR data. There is a single, symmetrical and broad (full width at half-height fwhh = 21 cm^{-1}) $^5D_0 \longrightarrow {}^7F_0$ transition at 17 226 cm^{-1}, which is consistent with the presence of a single europium(III) co-ordination environment. Using the phenomenological relationship of Frey and Horrocks[38] correlating the energy of the 0–0 transition and parameters describing the ability δ of co-ordinating atoms to produce a nephelauxetic effect, $\nu - \nu_0 = C_{CN}\Sigma_i n_i\delta_i$, and $\delta_{CO} = -15.7$, we find $\delta_{C\equiv N}(L^E) = -16.8$ cm^{-1}, a value somewhat larger than the averaged one deduced from our previous studies of complexes with heterocyclic imines, $\delta_{C\equiv N} = -15.3$.[26] The δ parameters are however very sensitive to bonding distances,[39] as shown for $[Eu_2(L^B)_3]^{6+}$ in the solid state for which three different metal ion sites were evidenced whose 0–0 transitions correspond to $\delta_{C\equiv N}$ parameters ranging from −13.7 to −18 cm^{-1}.[20] The large δ value obtained for the L^E helicate is nevertheless consistent with the large F_i values calculated for the H^3 and H^5 protons (see above) and pointing to an important spin delocalisation onto the pyridine ring.

The emission spectrum (*cf.* Table 7) may be interpreted in terms of a pseudo-D_3 symmetry, with a very weak $^5D_0 \longrightarrow {}^7F_0$ transition (forbidden in D_3 symmetry), two components for the transition to $^7F_1$ (allowed $A_1 \longrightarrow A_2$ and $A_1 \longrightarrow E$ transitions, the latter being split by distortion from the trigonal symmetry into two components spaced by 38 cm^{-1}) and two components for the transition to $^7F_2$ (two allowed $A_1 \longrightarrow E$ transitions). The $^5D_0$ lifetime, 1.62 ± 0.01 ms (Table 8), is long and identical to the one found for the helicate with L^B (1.67 ± 0.06 ms), consistent with fairly rigid metal ion sites.

Reinhoudt and co-workers[40] have concluded from their work on modified Eu^{III}-containing calix[4]arenes that the antenna effect is improved when the $^3\pi\pi^*$ 0-phonon transition lies 3500 cm^{-1} above the lanthanide excited state. They also observed that the $^1\pi\pi^* \longrightarrow {}^3\pi\pi^*$ intersystem crossing is maximised when the energy difference between these states amounts to *ca.* 5000 cm^{-1}. A similar conclusion was reached by Latva *et al.*,[39] finding that the best efficiency in energy transfer is obtained when the 0-phonon band of $^3\pi\pi^*$ lies at 21 000–22 000 cm^{-1}. Comparing the relative ability of L^B and L^E to sensitise europium(III) luminescence, we note the following facts: (i) the $^1\pi\pi^*$–$^3\pi\pi^*$

Table 7 Energy (cm^{-1}) of the $^5D_0$ and of the identified ^7F_J crystal field sublevels (origin: $^7F_0$) in the $[Eu_2(L^E)_3]^{6+}$ helicate from luminescence spectra at 10 (Eu-H10, Eu-H0, solid state) and 295 K (Eu-H0 in MeCN)

	Eu-H10			
	site Ia	site Ib	Eu-H0	10^{-3} M in MeCN
$^5D_0$	17 212	17 227	17 218	17 226
$^7F_1$	318	298	308	333
	374	386	383	390
	436	458	442	428
$^7F_2$	970	966	963 [a]	
	1 002	1 003	999 [b]	1 004
			1 005 [b]	
	1 044	1 045	1 053	1 094
	1 081	1 094	1 078	
	1 106	1124	1 103	
$^7F_3$	1 830	1 837	1 833	1 824
			1 866	
$^7F_4$	2 655			
	2 677	2 694	2 701	2 699
	2 724	2 739	2 722	2 735
	2 811	2 813	2 809	2 831
	2 880	2 897	2 880	2 900
	2 983	2 988	2 990	
	3 006	3 016		3 001

[a] Vibronic transition. [b] Splitting due to Fermi resonance (see text).

Table 8 Lifetimes of the Eu($^5D_0$) excited levels (ms) in the solid state samples of $[Eu_2(L^E)_3]^{6+}$ under various excitation conditions

Compound	T/K	ν_{exc}/cm^{-1}	τ/ms
Eu-H10	10	17 227	1.86 ± 0.01
		17 221	2.12 ± 0.01
		17 209	2.16 ± 0.02
	77	17 227	1.91 ± 0.02
		17 221	2.13 ± 0.01
		17 209	2.19 ± 0.01
	295	17 224	0.33 ± 0.02 [a]
			1.64 ± 0.01 [a]
Eu-H0	10	17 224	2.15 ± 0.01
		17 221	2.20 ± 0.01
		17 215	2.27 ± 0.01
		17 203	2.12 ± 0.04
	77	17 203	2.28 ± 0.03
		17 221	2.18 ± 0.01
	295	17 224	1.47 ± 0.01
[b]	295	17 227	1.62 ± 0.01

[a] Decomposition of bi-exponential decay. [b] $7 \cdot 10^{-4}$ M in dry deoxygenated CH_3CN.

energy difference amounts to 4510 (L^B) and 3600 cm^{-1} (L^E) but (ii) the 0-phonon transition of the ligand $^3\pi\pi^*$ state (as measured for the gadolinium complexes at 77 K) lies at 20 930 and 20 445 cm^{-1} for L^B and L^E, respectively, leading to $\Delta E(^3\pi\pi^*–{}^5D_0)$ differences equal to 3700 (L^B) and 3220 cm^{-1} (L^E). From these data one expects similar antenna effects in both helicates, which is observed: the absolute quantum yield of the metal-centred luminescence in acetonitrile amounts to 3.5×10^{-3} for L^B [20] and 4.4×10^{-3} for L^E. We note that these data parallel the results obtained for terbium(III) complexes with dipicolinates where the 4-Cl substituted compound proved to have better energy transfer efficiency than the unsubstituted complex.[23]

$[Ln_2(L^E)_3]^{6+}$ (Ln = Eu or Tb) helicates in the solid state. In complete contrast with the complexes of La, Gd and Lu, the emission from the ligand $^3\pi\pi^*$ state of helicates of Eu and Tb is completely quenched and the characteristic emission bands of the metal ions appear (Fig. 4). Since the europium helicate is fairly luminescent, we have investigated its high resolution emission spectra to gain information on the inner co-ordination sphere around the Eu^{III}. Furthermore, two samples were studied in order to unravel the influence of the hydration of the complex, one of them being anhydrous (Eu-H0) and the other one containing ten hydration water molecules (Eu-H10).

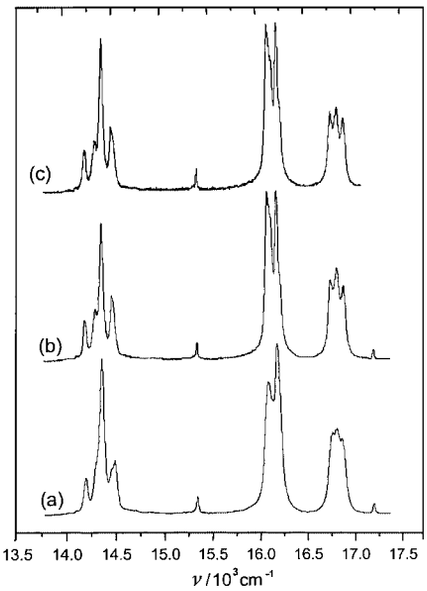

Fig. 5 Corrected emission spectra of anhydrous $[Eu_2(L^E)_3]^{6+}$ at 295 K: (a) $7 \cdot 10^{-3}$ M in CH_3CN, ν_{exc} = 25 316 cm^{-1}; (b) ν_{exc} = 25 000 cm^{-1}, solid state; (c) ν_{exc} = 17 226 cm^{-1}, solid state. Vertical scale: arbitrary units.

The emission spectrum of Eu-H0 recorded at 295 K under excitation through the ligand $^1\pi\pi^*$ state (Fig. 5) cannot simply be analysed in terms of a pseudo-D_3 symmetry, even if some of its characteristics are consistent with such a local symmetry at the co-ordination centre: (i) the $^5D_0 \longrightarrow {}^7F_0$ transition, which appears at 17 226 cm^{-1} is fairly broad (fwhh = 16 cm^{-1}), indicating some statistical distribution of europium(III) sites,[1] and it is quite weak (Table S5, supporting information), consistent with the fact that this transition is forbidden in D_3 symmetry; (ii) the transition to the $^7F_2$ level is comprised of two main bands (allowed $A_1 \longrightarrow E$ transitions), but these bands appear to be split; (iii) the $^5D_0 \longrightarrow {}^7F_4$ transition presents four lines, again consistent with D_3. On the other hand, the $^5D_0 \longrightarrow {}^7F_1$ transition comprises three almost equally spaced components, pointing to a low symmetry, since two transitions only are allowed in D_3. One of the latter being an $A_1 \longrightarrow E$ transition, slight deviations from the idealised D_3 symmetry lift the $^7F_1(E)$ degeneracy and often result in the observation of two lines for this transition. Here the distortion appears to be quite large with a splitting of 60–75 cm^{-1}. As a comparison, splittings in the range 20–30 cm^{-1} were observed for the helicate with L^B. To try to solve the ambiguity about the local symmetry at the europium(III) ion sites, we have recorded the $^5D_0 \longleftarrow {}^7F_0$ excitation spectrum. It consists of one relatively broad band (fwhh = 11–12 cm^{-1}) with a maximum at 17 218 and 17 223 cm^{-1} at 10 and 295 K, respectively, and a shoulder on the high energy side. Upon analysing at different emission wavelengths corresponding to transitions to $^7F_1$ and $^7F_2$, two additional components could be unravelled, at 17 228 and 17 209 cm^{-1}. However, the emission spectra recorded under excitation at the maximum of the emission band and in both shoulders are nearly identical (Fig. F1, Supporting Information), pointing to very similar metal-ion environments and suggesting that the additional shoulders appearing on the excitation spectra may be caused by vibronic transitions.[1,41] It could also be possible that the two metal ion sites are not completely identical within the same molecule or, even, as observed for $[Ln_2(L^C - 2H)_3]$, that two different types of molecules, with differing Ln···Ln distances, are present in the solid state. However, the crystal structures we have determined on several helicates have always shown that the two metal ion sites are fairly identical, differing

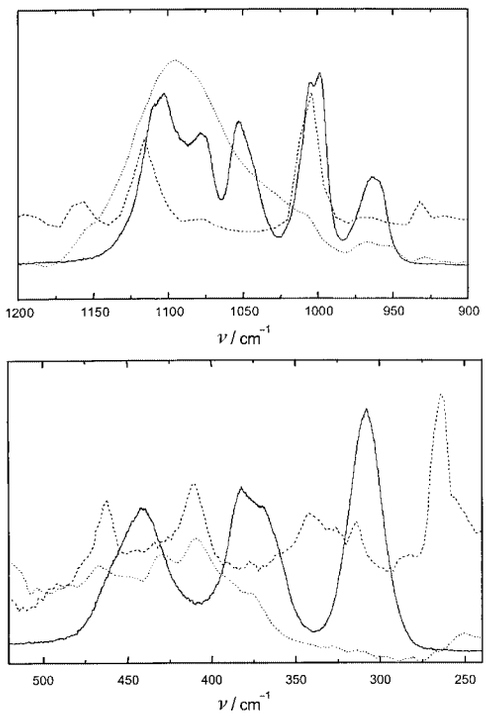

Fig. 6 Comparison between emission (solid line), IR (dotted line) and Raman (dashed line) spectra of $[Eu_2(L^E)_3]^{6+}$ in the energy range of the $^5D_0 \longrightarrow {}^7F_1$ (bottom) and $^5D_0 \longrightarrow {}^7F_2$ (top) transitions.

only by small distortions and slightly dissimilar Ln–O and Ln–N distances. This may cause a broadening but not a splitting of the luminescence bands. Developing further the hypothesis of an interaction with vibronic levels to explain the emission spectrum of $[Eu_2(L^E)_3]^{6+}$ we note that the highest energy $^5D_0 \longrightarrow {}^7F_1$ emission line undergoes a shift varying linearly with the excitation wavelength from 16 882 to 16 935 cm^{-1} (ν_{exc} = 17 209–17 227 cm^{-1}), as has been previously observed for a macrocyclic complex.[42] A correlation between the vibrational and emission spectra in the energy range of the transition to $^7F_1$ clearly shows interference with vibrational levels (Fig. 6). Therefore the large splitting observed for the $A_1 \longrightarrow E$ transition to the $^7F_1$ sublevel could arise from such an interaction.[43] Indeed, with respect to the energy of the $^5D_0$ level, the IR and Raman peaks at *ca.* 412 cm^{-1} fall in between the two $^7F_1$ sublevels with energy of 383 and 442 cm^{-1} which could therefore be the result of an interaction between a vibrational and an electronic state having very similar energy. Furthermore, at least six maxima can be identified in the $^5D_0 \longrightarrow {}^7F_2$ transition, but again there is an extensive interaction with the phonon density of states (Fig. 6), so that we interpret some closely spaced $^7F_2$ sublevels (Table 7) as resulting from interaction with vibrational levels, *e.g.* the levels at 999 and 1005 cm^{-1} (Raman band at 1005 cm^{-1}) or at 1078 and 1103 cm^{-1} (broad IR band at 1100 cm^{-1}, Raman peak at 1075 and 1120 cm^{-1}). Therefore, the emission spectrum of sample Eu-H0 can be interpreted as arising from two very similar europium(III) ions in a severely distorted pseudo-D_3 site symmetry, a conclusion reinforced by the fact that the Eu($^5D_0$) lifetime remains the same when the excitation energy is scanned through the $^5D_0 \longleftarrow {}^7F_0$ profile: 2.19 ± 0.07 ms (Table 8). The lifetime is long, as expected for an europium(III) environment free of OH oscillator but it is temperature dependent which points to vibrations interacting with the electronic levels of the metal ion and facilitating non-radiative de-excitation, in agreement with the above interpretation.

The $^5D_0 \longleftarrow {}^7F_0$ transition for the hydrated Eu-H10 sample presents a maximum at 17 221 cm^{-1} (10 K, fwhh between 13 and 17 cm^{-1} depending on the analysis wavelength) and two shoulders at 17 212 (site Ia) and 17 227 (site Ib) cm^{-1}. Excitation onto these two shoulders generates two slightly different emission spectra (see Table 7), while excitation at the maximum yields a spectrum which is a combination of the two other ones (Fig. F1, supporting information). The lifetime of site Ib (1.86 ms) is shorter than that of site Ia (2.16 ms, identical to the lifetime of the anhydrous sample). Both lifetimes are long, pointing to the absence of inner-sphere water molecules. Taking into account Δk = 0.15 ms^{-1} proposed by Beeby *et al.*[44] for the quenching effect of a closely diffusing unbound water molecule, we calculate that the lifetime difference corresponds to the presence of 0.5 H_2O in the outer co-ordination sphere of Eu(Ib). Upon increasing the temperature the lifetime of this site decreases much more drastically than the lifetime of site Ia, confirming larger vibronic interaction. Therefore, hydration of the helicate does not result in co-ordination of water in the inner sphere of the metal ion, but it generates non-covalent interactions with the ligand strands resulting in two slightly different metal ion sites. We cannot determine whether we are in the presence of two different types of molecules or of one type of unsymmetrical molecule. In the crystal structure of $[Ln_2(L^C - 2H)_3]\cdot 21.5H_2O$, not only two different types of molecules were observed, but within a dimetallic edifice, outer-sphere interaction with water molecules was found to be different for each metal ion site.[21]

The excitation spectrum of the terbium helicate at 77 K produces a broad band with a maximum at 25 814 cm^{-1}, corresponding to the excitation through the $^1\pi\pi^*$ ligand state. The corresponding emission spectrum displays $^5D_4 \longrightarrow {}^7F_J$ transitions at 20 362, 18 355, 17 101, 16 088 cm^{-1} for J = 6, 5, 4, and 3, respectively. It is dominated by the transition to $^7F_5$, as shown by the integrated and corrected relative intensities: 0.54, 1.00, 0.30 and 0.12 for J = 6, 5, 4 and 3. The lifetime of the $^5D_4$(Tb) state is short and sharply decreases from 1.10 ± 0.05 ms at 77 K to 0.122 ± 0.001 ms at 295 K, which is characteristic of a complex in which a $Tb^{III} \rightarrow L^E$ energy back transfer occurs as a result of the close proximity of the $^5D_4$ and $^3\pi\pi^*$ states, ΔE = 83 cm^{-1}, as was also observed for the helicate with L^B (ΔE = 70 cm^{-1}).[20] The luminescence decay of $[Tb_2(L^F)_3][ClO_4]_6$ is monoexponential with respect to temperature and an Arrhenius type plot yields an activation energy of 1410 ± 20 cm^{-1}, confirming the back-transfer mechanism.

Conclusion

The introduction of a chloride substituent in the 4 position of the pyridine rings of ligand L^B is straightforward and the resulting compound L^E is obtained in five steps with good overall yield, 32%, as calculated from the starting 4-hydroxypyridine-2,6-dicarboxylic acid. On the other hand, the bromide substituted ligand L^F, which is a more interesting synthon for further substitution at the 4 position of the pyridine, is more difficult to synthesize as indicated by an overall yield of 4–5% only. When treated with stoichiometric amounts of lanthanide perchlorates in acetonitrile, both ligands yield triple-stranded dimetallic helicates $[Ln_2(L)_3]^{6+}$ the stability of which is large (log β_{23} in the range 22–24) because the destabilising effect of the halogenide remains small. The structure of these edifices is very similar to the one determined for helicates with ligand L^B, pointing to the substitution not influencing the overall wrapping of the ligand strands around the two lanthanide ions. The electro-attracting chloride substituent in L^E results in a somewhat improved luminescence of the europium(III) ion over the helicate with the unsubstituted ligand, which demonstrates that tuning the efficiency of the ligand-to-metal energy transfer process may be achieved by varying the substituent at this position of the ligand. Moreover, the developed synthetic technology will enable us to graft coupling groups on this 4 position in order to produce bimetallic lanthanide-containing triple helicates able to combine with biological material[45] and therefore it opens the way to a whole series of new ditopic ligands for the design of luminescent (and magnetic) probes.

Experimental

Solvents and starting materials

Acetonitrile, dichloromethane, *N*,*N*-dimethylformamide (DMF), and triethylamine were distilled from CaH_2, thionyl chloride from elemental sulfur. Silica gel (Merck 60, 0.04–0.06 mm) was used for preparative column chromatography. Other products were purchased from Fluka AG (Buchs, Switzerland) and used without further purification, unless otherwise stated.

Spectroscopic and analytical measurements

Electronic spectra in the UV-vis range were recorded at 20 °C with a Perkin-Elmer Lambda 7 spectrometer using 1.0 and 0.1 cm quartz cells, reflectance spectra as finely ground powders dispersed in MgO (5%) with MgO as the reference on a Perkin-Elmer Lambda 900 spectrometer equipped with a Labsphere PELA-1000 integration sphere, IR spectra from KBr pellets with a Mattson α-Centauri FT-IR spectrometer and ES-MS spectra of the complexes on a Finnigan SSQ 710C spectrometer on 10^{-4} M solutions in acetonitrile (capillary temperature set to 200 °C and acceleration potential to 4.5 kV). ^{1}H and ^{13}C NMR spectra were recorded at 25 °C on Bruker AM-360 or AVANCE 400-DRX spectrometers. Chemical shifts are reported in parts per million with respect to TMS. Longitudinal ^{1}H relaxation times T_1 were measured by the inversion–recovery pulse sequence. The experimental procedures for high resolution, laser excited luminescence studies have been published previously.[20,46] Emission spectra were corrected for the instrumental functions, but high resolution excitation spectra were not. Quantum yields of the ligand centred emission were measured relative to quinine sulfate in diluted acidic solution (absolute quantum yield: 0.546).[47] Quantum yields of the metal-centred emission were determined as previously described[9e] at excitation wavelengths where (i) the Lambert–Beer law is obeyed and (ii) the absorption of the reference $[Eu(terpy)_3]^{3+}$ (absolute quantum yield 0.013)[24] closely matches that of the sample. Ligand excitation and emission spectra were recorded on a Perkin-Elmer LS-50B spectrometer equipped for low temperature (77 K) measurements. Elemental analyses were performed by Dr H. Eder (Microchemical Laboratory, University of Geneva).

Preparation of the ligands (Scheme 1)

4,4′-Bis(*N*-ethylamino)-3,3′-dinitrodiphenylmethane,[48] diethyl 4-bromopyridine-2,6-dicarboxylate[49] and L^{B}[20] were prepared as previously described.

4-Chloropyridine-2,6-dicarboxylic acid 1a. The product was prepared by the method of Robison.[50] Phenylphosphonic dichloride (50.41 g, 259 mmol) was added to 4-hydroxypyridine-2,6-dicarboxylic acid (13 g, 65 mmol), and the reaction mixture heated at 120 °C for 2 h under an inert atmosphere. After cooling, 200 mL of anhydrous methanol were added. The mixture was stirred vigorously for 1 h, concentrated to dryness and the residue dissolved in chloroform (200 mL). The solution was washed twice with water and twice with a half-saturated $NaHCO_3$ aqueous solution. The organic phase was dried over Na_2SO_4, filtered and evaporated to dryness. The residue was re-crystallised from methanol to obtain 12.78 g of dimethyl 4-chloropyridine-2,6-dicarboxylate (86% yield). ^{1}H NMR in $CDCl_3$: δ 4.00 (6 H, s) and 8.27 (2 H, s). ^{13}C NMR in $CDCl_3$: δ 54.05, 128.74, 147.31, 149.94 and 164.65. IR ν (cm^{-1}, KBr): 1728 (ν(C=O) ester). This ester (12.78 g, 55.6 mmol) was refluxed for 1 h in 250 mL of 5 M aqueous NaOH. After cooling, the solution was acidified to pH 2 with 25% aq. HCl. The white precipitate formed was filtered off and dried under vacuum to obtain 11 g of compound **1a** (98% yield). ^{1}H NMR in $CDCl_3$: δ 8.24 (2 H, s). ^{13}C NMR in DMSO-d_6: δ 130.39, 132.35, 149.38, 154.10 and 168.68. IR ν(cm^{-1}, KBr): 1722 (ν(C=O) acid) and 1575 (ν(C=C) py). ESI-MS(CH_3OH): *m*/*z* 201.9, $[M + H]^+$; and 401.0, $[2M + H]^+$.

4-Bromopyridine-2,6-dicarboxylic acid 1b. The compound was obtained by hydrolysis of diethyl 4-bromopyridine-2,6-dicarboxylate as described above for **1a** (90% yield). ^{1}H NMR in DMSO-d$_6$: δ 8.36 (2 H, s). ^{13}C NMR in DMSO-d_6: δ 134.15, 138.20, 153.64 and 168.42. ESI-MS (MeOH): *m*/*z* 266.0, $[M + H + H_2O]^+$. IR ν(cm^{-1}, KBr): 1732 (ν(C=O) acid) and 1571 (ν(C=N) py).

4-Chloro-6-methoxycarbonylpyridine-2-carboxylic acid 2a. To a solution of 4.0 g of compound **1a** (19.8 mmol) in water–MeOH (1 : 1) (70 mL), 2.5 mL of concentrated H_2SO_4 were added, and the resulting solution was refluxed for 30 min and then stirred for 12 h at room temperature. A saturated potassium bicarbonate aqueous solution (250 mL) was added and the mixture extracted with chloroform to remove all the diester (R_f = 0.81; CH_2Cl_2–MeOH 95 : 5). The aqueous phase was acidified to pH 2 with aq. HCl (25%) and extracted again with chloroform (4 × 150 mL). The combined organic phases were dried over Na_2SO_4 and evaporated to give 2.6 g of **2a** as a white solid (61% yield). ^{1}H NMR in $CDCl_3$: δ 4.04 (3 H, s, CH_3), 8.31 (1 H, d, ^4J = 1.94) and 8.39 (1 H, d, ^4J = 1.98 Hz). ^{13}C NMR in $CDCl_3$: δ 43.75, 130.81, 132.71, 149.44, 153.12, 154.53, 167.88 and 168.68. IR ν(cm^{-1}, KBr): 1707 (ν(C=O) ester), 1727 (ν(C=O) acid) and 1586 (ν(C=C) py). ESI-MS (MeOH): *m*/*z* 215.6, $[M + H]^+$.

4-Bromo-6-methoxycarbonylpyridine-2-carboxylic acid 2b. 9.46 g (38 mmol) of compound **1b** were dissolved in 200 mL of a 1 : 1 water–MeOH mixture and 3 mL of concentrated H_2SO_4 were added. The resulting solution was refluxed until complete dissolution of the carboxylic acid, stirred overnight at room temperature and then poured into 250 mL of a saturated $NaHCO_3$ solution. The mixture was then extracted with $CHCl_3$ to remove all the diester (R_f = 0.81, CH_2Cl_2–MeOH 95 : 5). The aqueous phase was acidified slowly to pH 2 with aq. HCl (37%) and extracted again with chloroform (5 × 100 mL). The combined organic phase was dried over Na_2SO_4 and evaporated to give 3.66 g of **2b** as a white solid (37% yield). ^{1}H NMR in $CDCl_3$: δ 4.05 (3 H, s, CH_3), 8.05 (1 H, d, ^4J = 1.94) and 8.32 (1 H, d, ^4J = 1.98 Hz). ESI-MS (MeOH): *m*/*z* 259.8, $[M + H]^+$. IR ν(cm^{-1}, KBr): 1706 (ν(C=O) ester), 1721 (ν(C=O) acid) and 1572 (ν(C=C) py).

4-Chloro-6-(*N*,*N*-diethylcarbamoyl)pyridine-2-carboxylic acid 3a. A 1.6 g (7.4 mmol) amount of compound **2a**, freshly distilled thionyl chloride (35.35 g, 297 mmol), and DMF (100 μL) were refluxed for 1 h in dry dichloromethane (30 mL) under an inert atmosphere. The yellow solid obtained after evaporation was pumped for 1 h (10^{-2} Torr) and dissolved in 30 mL of dry dichloromethane. 5.43 g (74.2 mmol) of diethylamine were added dropwise under an inert atmosphere. The solution was refluxed for 90 min and, after cooling, 150 mL of a half saturated NH_4Cl solution were added. The organic phase was separated and the aqueous phase extracted again with dichloromethane (2 × 100 mL). The combined organic phases were washed twice with 100 mL of a saturated $KHCO_3$ aqueous solution, dried over Na_2SO_4 and evaporated. The residue was dissolved in 100 mL of a 1 M KOH aqueous solution and the mixture refluxed for 30 min. The aqueous solution was extracted with dichloromethane (2 × 100 mL), acidified to pH 2 with aq. HCl (25%), and cooled at 0 °C for 12 h. The white crystals were collected by filtration to give 1.6 g of **3a** (6.2 mmol, yield 84%). ^{1}H NMR in $CDCl_3$: δ 1.26 (3H, t, ^3J = 7.00), 1.31 (3 H, t, ^3J = 7.00), 3.39 (2 H, q, ^3J = 7.00), 3.61 (2 H, q, ^3J = 7.00), 7.90 (1 H, d, ^4J = 1.76) and 8.24 (1 H, d, ^4J = 1.76 Hz). ^{13}C NMR in $CDCl_3$: δ 13.21, 14.62, 42.00, 45.19, 127.18, 127.42, 147.95, 150.52, 157.39, 166.52 and 168.78. IR ν(cm^{-1},

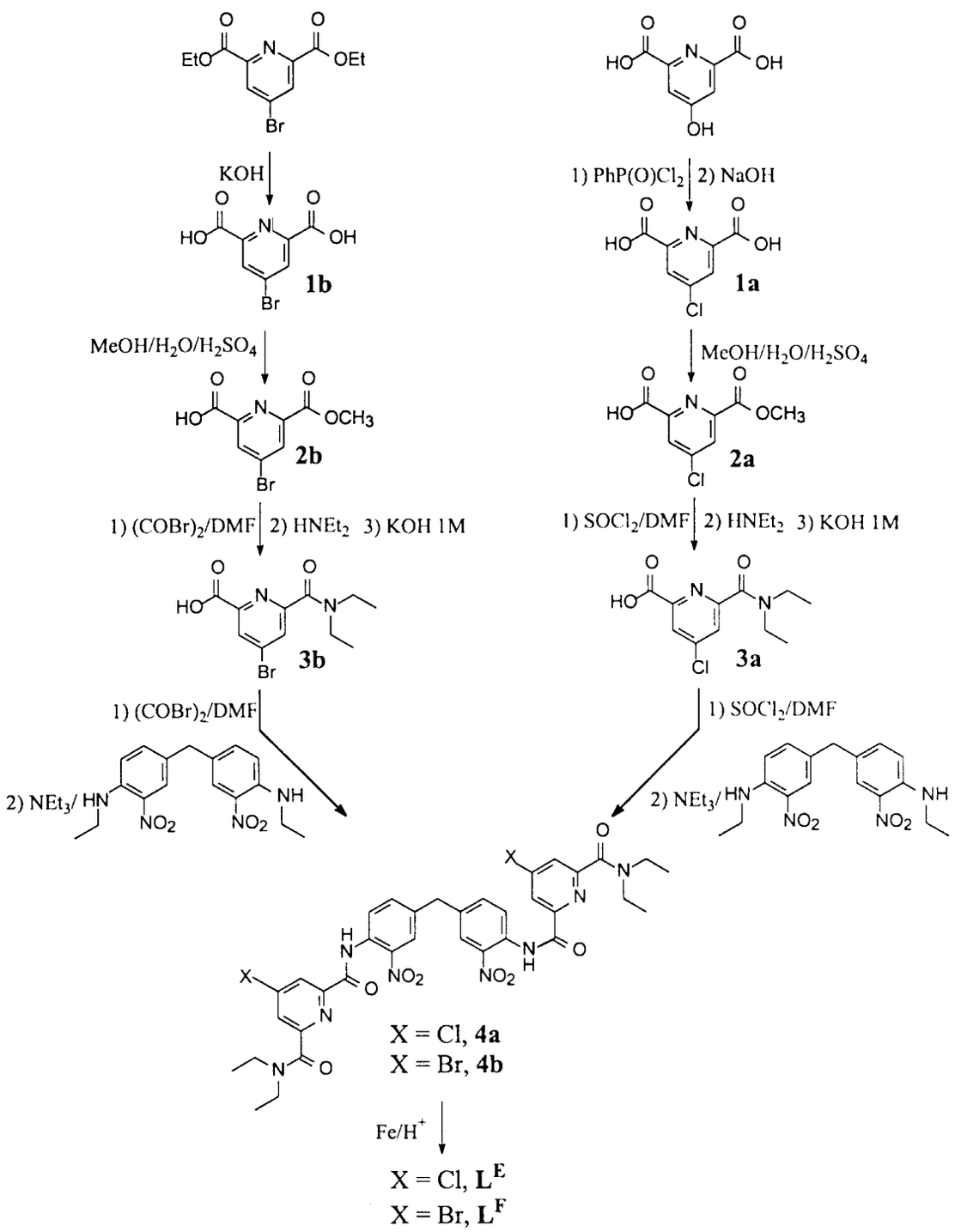

Scheme 1

KBr): 1607 (ν(C=O) amide), 1653 (ν(C=O) acid) and 1580 (ν(C=C) py). ESI-MS (MeOH): *m/z* 256.6, $[M + H]^+$.

4-Bromo-6-(*N*,*N*-diethylcarbamoyl)pyridine-2-carboxylic acid 3b. A 2.59 g (9.97 mmol) amount of compound **2b** was dissolved in 60 mL of dry toluene under an inert atmosphere (N_2) and 6.45 g (30 mmol) of $(COBr)_2$ and 100 μL of DMF were added slowly. The resulting solution was vigorously stirred for 1 h and then heated to 70 °C for 2 h. The brown solid obtained after evaporation was pumped for 1 h (10^{-2} Torr) and dissolved in 30 mL of dry dichloromethane. 7.03 g (99.7 mmol) of diethylamine were added dropwise under an inert atmosphere. The solution was refluxed under nitrogen for 90 min and, after cooling, 100 mL of CH_2Cl_2 were added. The solution was washed with water (2 × 100 mL). The combined organic phases were dried over anhydrous Na_2SO_4. The resulting product was dried under vacuum (10^{-2} Torr) at 50 °C to get 2.5 g (7.9 mmol) of methyl 4-bromo-6-(*N*,*N*-diethylcarbamoyl)pyridine-2-carboxylate (yield 79%). ^{1}H NMR in $CDCl_3$: δ 1.25 (6 H, t, $^3J = 7.02$), 3.38 (2 H, q, $^3J = 7.02$), 3.53 (2 H, q, $^3J = 7.02$), 3.98 (3 H, s), 8.00 (1 H, d, $^4J = 1.72$) and 8.28 (1 H, d, $^4J = 1.44$ Hz). The product was dissolved in 100 mL of a 1 M KOH aqueous solution and the mixture refluxed for 2 h and acidified to pH 2 with aq. HCl (37%). A white precipitate formed which was collected by filtration to give 2.27 g (7.53 mmol) of **3b** (overall yield 76%). ^{1}H NMR in $CDCl_3$: δ 1.22 (3 H, t, $^3J = 6.96$), 1.29 (3 H, t, $^3J = 7.16$), 3.32 (2 H, q, $^3J = 7.09$), 3.58 (2 H, q, $^3J = 7.09$), 8.00 (1 H, d, $^4J = 1.84$) and 8.40 (1 H, d, $^4J = 1.84$ Hz). ^{13}C NMR in $CDCl_3$: δ 13.38, 15.10, 41.12, 43.99, 128.70, 131.10, 137.0, 146.6, 155.3, 163.3 and 166.2. ESI-MS (MeOH):

m/z 302.7, $[M + H]^+$. IR ν(cm^{-1}, KBr): 1598 (ν(C=O) amide), 1713 (ν(C=O) acid) and 1566 (ν(C=C) py).

Compound 4a. A 1.14 g (4.7 mmol) amount of compound **3a**, thionyl chloride (16.78 g, 141 mmol), and DMF (100 μL) were refluxed for 90 min in dry dichloromethane (50 mL) under an inert atmosphere. The solution was concentrated to dryness and the residue dried under vacuum for 30 min. This was dissolved in 30 mL of dry dichloromethane and a 30 mL solution of 4,4′-bis(*N*-ethylamino)-3,3′-dinitrodiphenylmethane (0.80 g, 2.4 mmol) and triethylamine (47 mmol) was added dropwise. The resulting solution was stirred at room temperature for 2 h and refluxed during 4 h under an inert atmosphere. Upon evaporation a brown residue was obtained. This was partitioned between dichloromethane (3 × 100 mL) and half-saturated NH_4Cl (100 mL) solution. The combined organic phases were dried over Na_2SO_4 and evaporated, and the resulting crude residue was purified by column chromatography (silica gel; CH_2Cl_2 to CH_2Cl_2–MeOH 99 : 1), to yield 1.50 g of **4a** (78% yield). ^1H NMR in $CDCl_3$: δ 0.78–1.42 (18 H, m), 2.81–3.68 (12 H, m), 4.01–4.42 (2 H, m) and 6.98–7.98 (10 H, m). ESI-MS (MeOH): *m/z* 821.6, $[M + H]^+$; and 843.5, $[M + Na]^+$. IR ν(cm^{-1}, KBr): 1533 (ν(C=C)), 1349, 1568 (NO_2), 1645 (ν(C=O)).

Compound 4b. A 1.60 g (5.32 mmol) amount of compound **3b** and 40 mL of dry toluene were mixed under an inert atmosphere (N_2) and 3.48 g (16 mmol) of $(COBr)_2$ and 100 μL of DMF were slowly added. The resulting solution was vigorously stirred for 1 h and then heated to 70 °C for 2 h. The solid obtained after evaporation was pumped for 30 min (10^{-2} Torr) and dissolved in 30 mL of dry dichloromethane. A solution of 4,4′-bis(*N*-ethylamino)-3,3′-dinitrodiphenylmethane (0.80 g, 2.4 mmol) and triethylamine (47 mmol) in the same solvent (40 mL) was added dropwise. The resulting solution was stirred at room temperature for 2 h, refluxed during 4 h under an inert atmosphere and evaporated. The brown residue was partitioned between dichloromethane (3 × 100 mL) and a half-saturated NH_4Cl (100 mL) solution. The combined organic phases were dried over Na_2SO_4 and evaporated, and the resulting crude residue was purified by column chromatography (silica gel; CH_2Cl_2 to CH_2Cl_2–MeOH 98.5 : 1.5, R_f = 0.40 in CH_2Cl_2–MeOH 97 : 3), to yield 0.60 g (0.66 mmol) of **4b** (yield 24.8%). ^1H NMR in $CDCl_3$: δ 0.75–1.38 (18 H, m), 2.85–3.62 (12 H, m), 4.05–4.45 (2 H, m) and 7.03–8.01 (10 H, m). ESI-MS (MeOH): *m/z* 911.2, $[M + H]^+$; and 456.5, $[M + 2H]^{2+}$. IR ν(cm^{-1}, KBr): 1533 (ν(C=C)), 1345, 1566 ($\nu(NO_2)$), 1644 (ν(C=O)).

Bis{1-ethyl-2-[4-chloro-6-(*N*,*N*-diethylcarbamoyl)pyridin-2-yl]benzimidazol-5-yl}methane (L^E). Freshly activated iron powder (2.85 g, 51 mmol) and HCl (25%, 16.53 g, 118.5 mmol) were added to a solution of compound **4a** (1.30 g, 1.58 mmol) in EtOH–water (220 : 56 mL). The mixture was refluxed overnight under an inert atmosphere. The golden coloured solution was cooled, filtered and evaporated to remove the ethanol. $Na_2H_2EDTA{\cdot}2H_2O$ (31.76 g, 85.32 mmol) in 100 mL of water and 100 mL of CH_2Cl_2 were added to the mixture and the pH of the aqueous phase was adjusted to 7 using aq. NaOH (25%). H_2O_2 (30%, 1 mL) was added to the aqueous phase and the pH adjusted to 8.5. The two phases underwent vigorous stirring before separation and the aqueous phase was extracted with CH_2Cl_2 (5 × 100 mL). The combined organic phases were dried over Na_2SO_4, filtered, and evaporated to dryness, resulting in a pale brown solid which was purified by column chromatography (silica gel; CH_2Cl_2 to CH_2Cl_2–MeOH 98 : 2, R_f = 0.48 in CH_2Cl_2–MeOH 95 : 5) to give 0.95 g of L^E as a pale yellow solid (yield 83%) [Found: C, 64.35; H, 5.87; N, 15.29. Calc. for $C_{39}H_{42}Cl_2N_8O_2$: C, 64.55; H, 5.83; N, 15.44%]. ^1H NMR in $CDCl_3$: δ 1.08 (3 H, t, ^3J = 7.04), 1.26 (3 H, t, ^3J = 7.08), 1.42 (3 H, t, ^3J = 6.98), 3.35 (2 H, q, ^3J = 6.96), 3.59 (2 H, q, ^3J = 6.97), 4.27 (1 H, s), 4.72 (2 H, q, ^3J = 6.72), 7.24 (1 H, d, ^3J = 8.32), 7.35 (1 H, d, ^3J = 8.4), 7.52 (1 H, d, ^4J = 1.72), 7.67 (1H, s), 8.42 (1 H, d, ^4J = 1.8 Hz). ^{13}C NMR in $CDCl_3$: δ 13.42, 14.98, 16.07, 40.30, 41.26, 42.84, 43.48, 110.78, 120.86, 123.37, 125.64, 126.06, 135.62, 137.35, 143.71, 146.64, 148.73, 151.53, 156.29 and 167.96. IR ν (cm^{-1}, KBr): 1561 (ν(C=C)) and 1635 (ν(C=O)). ESI-MS (MeOH): *m/z* 725.3, $[M + H]^+$.

Bis{1-ethyl-2-[4-bromo-6-(*N*,*N*-diethylcarbamoyl)pyridin-2-yl]benzimidazol-5-yl}methane (L^F). Freshly activated iron powder (1.08 g, 19.3 mmol) and HBr (47%, 8.32 g, 48.7 mmol) were added to a solution of compound **4b** (0.59 g, 0.65 mmol) in EtOH–water (111 : 28 mL). The mixture was refluxed for three days under an inert atmosphere. The resulting solution was cooled, filtered and evaporated to remove the ethanol. $Na_2H_2EDTA{\cdot}2H_2O$ (13.2 g) in 100 mL of water and 100 mL of CH_2Cl_2 were added and the pH of the aqueous phase was adjusted to 7 using aqueous NH_4OH (12%). H_2O_2 (30%, 1 mL) was added to the aqueous phase and the pH adjusted to 8.5. The two phases were vigorously stirred before separation and the aqueous phase was extracted with CH_2Cl_2 (6 × 100 mL). The combined organic phases were dried over Na_2SO_4, filtered, and evaporated to dryness, resulting in a yellow-orange solid which was purified by column chromatography (silica gel; CH_2Cl_2 to CH_2Cl_2–MeOH 99 : 1; R_f = 0.32 in CH_2Cl_2–MeOH 97 : 3) to give 0.35 g (0.43 mmol) of L^F as a pale green solid (yield 66%) [Found: C, 57.51; H, 5.25; N, 13.65. Calc. for $C_{39}H_{42}Br_2N_8O_2$: C, 57.50; H, 5.20; N, 13.76%]. ^1H NMR in $CDCl_3$: δ 1.10 (3 H, t, ^3J = 7.04), 1.28 (3 H, t, ^3J = 7.08), 1.43 (3 H, t, ^3J = 6.98), 3.36 (2 H, q, ^3J = 6.96), 3.59 (2 H, q, ^3J = 6.97), 4.29 (1 H, s), 4.74 (2 H, q, ^3J = 6.72), 7.26 (1 H, d, ^3J = 8.32), 7.35 (1 H, d, ^3J = 8.4), 7.68 (1 H, d, ^4J = 1.72), 7.79 (1 H, s) and 8.60 (1 H, d, ^4J = 1.8 Hz). ESI-MS (MeOH): *m/z* 815.2, $[M + H]^+$; and 408.4, $[M + 2H]^{2+}$. IR ν(cm^{-1}, KBr): 1558 (ν(C=C)) and 1639 (ν(C=O)).

Preparation of the complexes

The perchlorate salts $Ln(ClO_4)_3{\cdot}nH_2O$ (Ln = La to Lu, except Pm; n = 6–8) were prepared from the corresponding oxides (Rhône-Poulenc, 99.99%) according to the literature method.[51] $Eu(ClO_4)_3$ was prepared from $Eu(ClO_4)_3{\cdot}nH_2O$ ($n \approx 2$) by slowly increasing the temperature from 30 to 80 °C under vacuum.[52] **CAUTION**: perchlorate salts combined with organic ligands are potentially explosive and should be handled in small quantity and with the necessary precautions.[53]

$[Ln_2(L^E)_3][ClO_4]_6{\cdot}nH_2O$ (Ln = La, Eu, Gd, Tb or Lu). A 22.97 μmol amount of $Ln(ClO_4)_3{\cdot}nH_2O$ in dry acetonitrile (1.5 mL) was slowly added to a solution of L^E (25 mg, 34.45 μmol) in dry dichloromethane (1 mL). After stirring at room temperature for 2 h the solution was evaporated, the solid residue re-dissolved in acetonitrile (1 mL), solution was filtered, and diethyl ether diffused into the solution for 2–3 days. The resulting pale yellow microcrystalline aggregates were collected by filtration and dried to give the complexes $[Ln_2(L^E)_3][ClO_4]_6{\cdot}nH_2O$ (Ln = La (n = 10), Eu (10), Gd (4), Tb (7) or Lu (8) in 65–76% yields. The $[Ln_2(L^E)_3]^{6+}$ (Ln = Pr, Nd, Sm, Dy, Ho, Er, Tm or Yb) complexes for NMR measurements were prepared by the same procedure but not recrystallised.

Anhydrous $[Eu_2(L^E)_3][ClO_4]_6$. A 25 μmol amount of anhydrous $Eu(ClO_4)_3$ in dry acetonitrile (1.5 mL) was slowly added to a solution of L^E (27.2 mg, 37.5 μmol) in dry dichloromethane (1 mL). After being stirred at room temperature for 2 h the solution was evaporated to dryness. The solid residue was dissolved in dry acetonitrile (1 mL), the solution filtered in a glove-box, and dry THF diffused into the solution for 24 h. The resulting pale yellow microcrystalline aggregates were collected by filtration and dried to give $[Eu_2(L^E)_3][ClO_4]_6$ (yield 80%).

Acknowledgements

This work is supported by grants from the Swiss National Science Foundation and by the Swiss Office for Education and Science (COST action D18). We thank Veronique Foiret and Gaël Zucchi for their help in recording high resolution luminescence spectra and lifetimes.

References

1 J.-C. G. Bünzli, in *Rare Earths*, eds. R. Saez-Puche and P. Caro, Editorial Complutense, Madrid, 1998, p. 223ff.
2 R. B. Lauffer, in *MRI Clinical Magnetic Resonance Imaging*, eds. R. R. Edelman, M. B. Zlatkin and J. R. Hesselink, W. B. Saunders Co., Philadelphia, 2nd edn., 1996, vol. 1, ch. 5; P. Caravan, J. J. Ellison, T. J. McMurry and R. B. Lauffer, *Chem. Rev.*, 1999, **99**, 2293.
3 T. C. Bruice, A. Tsubouchi, R. O. Dempcy and L. P. Olson, *J. Am. Chem. Soc.*, 1996, **118,** 9867; P. Hurst, B. K. Takasaki and J. Chin, *J. Am. Chem. Soc.*, 1996, **118**, 9982.
4 G. L. DeNardo, G. R. Mirik, L. A. Kroger, R. T. O'Donnel, C. F. Meares and S. J. De Nardo, *J. Nucl. Med.*, 1996, **37**, 451; M. J. Heeg and S. S. Jurisson, *Acc. Chem. Res.*, 1999, **32**, 1053.
5 J.-C. G. Bünzli, in *Lanthanide Probes in Life, Chemical and Earth Science*, eds. J.-C. G. Bünzli and G. R. Choppin, Elsevier Science Publ. B.V., Amsterdam, 1989, ch. 7.
6 *Biomedical Applications of Labelling Technologies*, eds. I. Hemmilä, T. Ståhlberg and P. Mottram, Wallac Oy, Turku, 2nd edn., 1995; G. Mathis, in *Rare Earths*, eds. R. Saez-Puche and P. Caro, Editorial Complutense, Madrid, 1998.
7 S. Aime, A. Barge, M. Botta, J. A. K. Howard, R. Kataky, M. P. Lowe, J. M. Moloney, D. Parker and A. S. de Sousa, *Chem. Commun.*, 1999, 1047.
8 N. Sabbatini, S. Perathoner, V. Balzani, B. Alpha and J.-M. Lehn, in *Supramolecular Chemistry*, ed. V. Balzani, Reidel Publishing Co., Dordrecht, 1987.
9 (*a*) G. Blasse, *Phys. Status Solidi A*, 1992, **130**, K85; (*b*) J.-C. G. Bünzli, P. Froidevaux and J. M. Harrowfield, *Inorg. Chem.*, 1993, **32**, 3306; (*c*) S. Petoud, T. Glanzmann, J.-C. G. Bünzli, C. Piguet, X. Qin and R. P. Thummel, *J. Luminesc.*, 1999, **82**, 69.
10 V. Alexander, *Chem. Rev.*, 1995, **95**, 273; J.-C. G. Bünzli, F. Ihringer and F. Besançon, *ACS Symp. Ser.*, 2000, **14**.
11 J.-C. G. Bünzli, N. André, M. Elhabiri, G. Muller and C. Piguet, *J. Alloys Compd.*, 2000, **303/304**, 66.
12 P. L. Jones, A. J. Amoroso, J. C. Jeffery, J. A. McCleverty, E. Psillakis, L. H. Rees and M. D. Ward, *Inorg. Chem.*, 1997, **36**, 10; N. Armaroli, G. Accorsi, F. Barigelletti, S. M. Couchman, J. S. Fleming, N. C. Harden, J. C. Jeffery, K. L. V. Mann, J. A. McCleverty, L. H. Rees, S. R. Starling and M. D. Ward, *Inorg. Chem.*, 1999, **38.** 5769; F. Renaud, C. Piguet, G. Bernardinelli, G. Hopfgartner and J.-C. G. Bünzli, *Chem. Commun.*, 1999, 457; C. Piguet, C. Edder, H. Nozary, F. Renaud, S. Rigault and J.-C. G. Bünzli, *J. Alloys Compd.*, 2000, **303/304**, 94.
13 J.-M. Lehn, *Supramolecular Chemistry. Concepts and Perspectives*, VCH, Weinheim, 1995.
14 C. Piguet and J.-C. G. Bünzli, *Chem. Soc. Rev.*, 1999, **28**, 347.
15 D. E. Koshland, Jr., *Angew. Chem.*, *Int. Ed. Engl.*, 1994, **33**, 2375.
16 (*a*) C. Piguet, E. Rivara-Minten, G. Hopfgartner and J.-C. G. Bünzli, *Helv. Chim. Acta*, 1995, **78**, 1541; (*b*) C. Piguet, J.-C. G. Bünzli, G. Bernardinelli, G. Hopfgartner, S. Petoud and O. Schaad, *J. Am. Chem. Soc.*, 1996, **118**, 6681; (*c*) C. Edder, C. Piguet, J.-C. G. Bünzli and G. Hopfgartner, *J. Chem. Soc.*, *Dalton Trans.*, 1997, 4657.
17 C. Piguet, E. Rivara-Minten, G. Hopfgartner and J.-C. G. Bünzli, *Helv. Chim. Acta*, 1995, **78**, 1651; C. Piguet, E. Rivara-Minten, G. Bernardinelli, J.-C. G. Bünzli and G. Hopfgartner, *J. Chem. Soc.*, *Dalton Trans.*, 1997, 421.
18 S. Rigault, C. Piguet, G. Bernardinelli and G. Hopfgartner, *Angew. Chem.*, *Int. Ed. Engl.*, 1988, **27**, 169.
19 C. Piguet, J.-C. G. Bünzli, G. Bernardinelli, G. Hopfgartner and A. F. Williams, *J. Am. Chem. Soc.*, 1993, **115**, 8197.
20 N. Martin, J.-C. G. Bünzli, V. McKee, C. Piguet and G. Hopfgartner, *Inorg. Chem.*, 1998, **37**, 577.
21 M. Elhabiri, R. Scopelliti, J.-C. G. Bünzli and C. Piguet, (*a*) *Chem. Commun.*, 1998, 2347; (*b*) *J. Am. Chem. Soc.*, 1999, **121**, 10747.
22 K. Sonogashira, Y. Tohda and N. Hagihara, *Tetrahedron Lett.*, 1975, **50**, 4467; H. A. Dieck and F. R. Heck, *J. Organomet. Chem.*, 1975, **93**, 259.
23 J. B. Lamture, Z. Hong Zhou, A. S. Kumar and T. G. Wensel, *Inorg. Chem.*, 1995, **34**, 864.
24 C. Platas, F. Avecilla, A. de Blas, C. F. G. C. Geraldes, T. Rodriguez-Blas, H. Adams and J. Mahia, *Inorg. Chem.*, 1999, **38**, 3190.
25 S. Rigault, C. Piguet and J.-C. G. Bünzli, *J. Chem. Soc.*, *Dalton Trans.*, 2000, DOI: 10.1039/b000147n.
26 S. Petoud, J.-C. G. Bünzli, K. J. Schenk and C. Piguet, *Inorg. Chem.*, 1997, **36**, 1345.
27 K. Nakamoto, *Infrared and Raman Spectra of Inorganic and Co-ordination Compounds*, J. Wiley, New York, 3rd edn., 1972, pp. 142–154.
28 I. Marolleau, J. P. Gisselbrecht, M. Gross, F. Arnaud-Neu and M. J. Schwing-Weill, *J. Chem. Soc.*, *Dalton Trans.*, 1990, 1285.
29 J. A. Peters, J. Huskens and D. J. Raber, *Prog. NMR Spectrosc.*, 1996, **28**, 283.
30 A. D. Sherry and C. F. G. C. Geraldes, in *Lanthanide Probes in Life, Chemical and Earth Sciences*, eds. J.-C. G. Bünzli and G. R. Choppin, Elsevier Science Publ. B.V., Amsterdam, 1989, ch. 4.
31 C. N. Reilley, B. W. Good and J. F. Desreux, *Anal. Chem.*, 1975, **47**, 2110.
32 R. M. Golding and M. P. Halton, *Aust. J. Chem.*, 1972, **25**, 2577; A. A. Pinkerton, M. Rossier and S. Stavros, *J. Magn. Reson.*, 1985, **64**, 420.
33 B. Bleaney, *J. Magn. Reson.*, 1972, **8**, 91.
34 J. Ren and D. Sherry, *J. Magn. Reson.*, 1996, **B111**, 178.
35 M. D. Kemple, B. D. Ray, K. B. Lipkowitz, F. G. Prendergast and B. N. D. Rao, *J. Am. Chem. Soc.*, 1988, **110**, 8275.
36 J. Lisowski, J. L. Sessler, V. Lynch and T. D. Moody, *J. Am. Chem. Soc.*, 1995, **117**, 2273; J. Lisowski, *Magn. Reson. Chem.*, 1999, **37**, 287.
37 V. Clementi and C. Luchinat, *Acc. Chem. Res.*, 1998, **31**, 351; S. Aime, M. Botta, D. Parker and J. A. G. Williams, *J. Chem. Soc.*, *Dalton Trans.*, 1995, 2259.
38 S. T. Frey and W. de W. Horrocks, Jr., *Inorg. Chim. Acta*, 1995, **229**, 384.
39 M. Latva, H. Takalo, V. M. Mukkala, C. Matachescu, J.-C. Rodriguez-Ubis and J. Kankare, *J. Luminesc.*, 1997, **75**, 149.
40 F. J. Steemers, W. Verboom, D. N. Reinhoudt, E. B. Vandertol and J. W. Verhoeven, *J. Am. Chem. Soc.*, 1995, **117**, 9408.
41 C. Platas, F. Avecilla, A. de Blas, T. Rodriguez-Blas, C. F. G. C. Geraldes, E. Toth, A. E. Merbach and J.-C. G. Bünzli, *J. Chem. Soc.*, *Dalton Trans.*, 2000, 611.
42 G. Zucchi, R. Scopelliti, P.-A. Pittet, J.-C. G. Bünzli and R. D. Rogers, *J. Chem. Soc.*, *Dalton Trans.*, 1999, 931.
43 J.-C. G. Bünzli, B. Klein, D. Wessner and N. W. Alcock, *Inorg. Chim. Acta*, 1982, **59**, 269; J.-C. G. Bünzli, G. A. Leonard, D. Plancherel and G. Chapuis, *Helv. Chim. Acta*, 1986, **69**, 288.
44 A. Beeby, I. M. Clarkson, R. S. Dickins, S. Faulkner, D. Parker, L. Royle, A. S. de Sousa, J. A. G. Williams and M. Woods, *J. Chem. Soc.*, *Perkin Trans. 2*, 1999, 493.
45 M. Hollenstein, Diploma Thesis, University of Lausanne, 1999.
46 C. Piguet, A. F. Williams, G. Bernardinelli, E. Moret and J.-C. G. Bünzli, *Helv. Chim. Acta*, 1992, **75**, 1697.
47 S. R. Meech and D. Phillips, *J. Photochem.*, 1983, **23**, 193.
48 C. Piguet, G. Bernardelli, B. Bocquet, A. Quattropani and A. F. Williams, *J. Am. Chem. Soc.*, 1992, **114**, 7440.
49 H. Takalo and J. Kankare, *Acta Chem. Scand.*, *Ser. B*, 1987, **41**, 219; B. Schmidt and D. Ehlert, *Tetrahedron Lett.*, 1998, **39**, 3999.
50 M. H. Robison, *J. Am. Chem. Soc.*, 1958, **80**, 5481; B. Pitteri, L. Cattalini, G. Chessa, G. Marangoni, N. Stevanato and M. L. Tobe, *J. Chem. Soc.*, *Dalton Trans.*, 1991, 3049.
51 J. F. Desreux, in *Lanthanide Probes in Life, Chemical and Earth Sciences*, eds. J.-C. G. Bünzli and G. R. Choppin, Elsevier Science Publ. B.V., Amsterdam, 1989, ch. 2.
52 J.-C. G. Bünzli, J.-R. Yersin and C. Mabillard, *Inorg. Chem.*, 1982, **21**, 1471.
53 W. C. Wolsey, *J. Chem. Educ.*, 1973, **50**, A335.